The Pennsylvania State University

The Graduate School

ANTIBODY RETENTION AND FLUX DECLINE DURING FILTRATION THROUGH VIRUS RETENTIVE MEMBRANES

A Thesis in

Chemical Engineering

by

Matthew William Billups

Submitted in Partial Fulfillment
of the Requirements
for the Degree of

Master of Science

August 2021

The thesis of Matthew William Billups was reviewed and approved by the following:

Andrew Zydney
Bayard D. Kunkle Chair and Professor of Chemical Engineering
Thesis Advisor

Ali Borhan
Professor of Chemical Engineering

Stephanie Butler Velegol
Associate Teaching Professor of Chemical Engineering

Hee Jeung Oh
Assistant Professor of Chemical Engineering

Phillip Savage
Walter L. Robb Family Chair
Head of the Department of Chemical Engineering

ABSTRACT

Virus filtration is a key component of the overall virus clearance strategy in the production of monoclonal antibodies. These virus filtration membranes also provide one of the most selective membrane separations ever demonstrated, with more than 95% recovery of the antibody product in the filtrate with more than 99.99% retention of even small parvovirus, despite the less than 2-fold difference in size between the virus and antibody. However, the filtrate flux through these virus filters can often decrease by more than 100-fold during filtration of these antibody solutions. The objectives of this thesis were to obtain a more quantitative understanding of the intrinsic sieving characteristics and filtrate flux behavior of commercially available virus filters.

Experiments were performed with the Viresolve® Pro and Pegasus™ SV4 virus filters both with and without stirring to control the effects of concentration polarization. The actual sieving coefficient of a highly purified monoclonal antibody was less than 0.05 for both membranes, demonstrating that the high antibody recovery during typical virus filtration processes is a direct result of the high degree of concentration polarization in these systems. The intrinsic selectivity of the virus filter was in good agreement with predictions of available hydrodynamic models accounting for a log-normal pore size distribution. The actual sieving coefficient also decreased with increasing antibody concentration, consistent with available models for proteins with attractive interactions (negative values of the interaction parameter).

The filtrate flux was found to be a strong function of antibody properties, with very low flux for more hydrophobic antibodies that show significant intermolecular attractive interactions. Filtrate flux data were obtained with the asymmetric Viresolve® Pro filter in both orientations, selective skin-up and skin-down, and in combination with different prefilters. The Viresolve® Pro had much higher flux during filtration with the skin-side down, demonstrating the importance

of orientation on the virus filter behavior. The use of large pore size prefilters upstream of the Viresolve® Pro skin significantly improved the flux behavior when the filter was oriented skin-side down, but only when the pre-filter was placed directly on top of the Viresolve® Pro. This 100-fold improvement in flux was not seen after batch prefiltration. Data obtained using an in-line prefiltration demonstrated that the critical factor was the residence time between the prefilter and the Viresolve® Pro, suggesting that the prefilter disrupts small aggregates in the antibody solution that then reversibly self-associate leading to a reduction in filtrate flux. This behavior is consistent with the presence of strong intermolecular attractive interactions in these antibody solutions. These results provide important insights into the transport characteristics of virus filters and their effect on the performance of these virus filters in bioprocessing.

TABLE OF CONTENTS

LIST OF FIGURES

LIST OF TABLES

ACKNOWLEDGEMENTS

First, I want to thank Dr. Zydney for being my advisor and providing the opportunity to work in his lab. His encouragement to try new things, patience when things did not go as planned and guidance while trying to navigate challenging and complex situations makes him a very special advisor.

Next, this research project would not have existed without the team at Bristol Myers Squibb from Devens, Massachusetts and New Brunswick, New Jersey. Melissa Holstein, Hasin Feroz, Swarnim Ranjan, Jessica Hung, Haiying Bao, Sanchayita Ghose and Zheng Jian Li all had significant contributions to the progression of this work, whether that be in the form of supplying the materials, providing us supplemental data, intellectual and troubleshooting discussions, or acquiring and advocating for funding this collaboration.

To the members of this thesis committee, Dr. Ali Borhan, Dr. Stephanie Velegol, and Dr. Hee Jung Oh. Your experience and feedback is greatly appreciated in evaluating this work, ensuring it has the breadth and depth to well represent the Chemical Engineering Department at Penn State Univeristy.

Zydney lab members, Fatemeh, Parinaz, Ivan, Zhao, Mario, Negin, Chris, Kait, Neil, Josh and Vikram. Our daily interactions, or brainstorming/venting sessions are what helped motivate me to overcome technical challenges and broaden my research perspective. Special recognition to Mirko for helping conduct many filtration experiments and also to Andrew, for helping with experiments, especially during the modified lab scheduling.

To my family and friends, I am forever grateful for their support during this endeavor, especially my parents and brother, who have always been my biggest supporters.

Finally, I would like to acknowledge my partner, Julia. She has experienced it all from behind the scenes and her love and support for me has never wavered. I am truly grateful she has been by my side during this journey.

Chapter 1

Introduction

1.1 Pharmaceutical bioprocessing and virus filtration

As the therapeutic use of monoclonal antibodies (mAbs) for the treatment of historically difficult to treat diseases has become a major factor in today's healthcare (Sommerfeld and Strube 2005) . Monoclonal antibodies serve as treatments for various diseases such as cancer, auto-immune diseases and infectious diseases. For instance, monoclonal antibodies can neutralize an aberrant signaling pathway through competitive inhibition. By binding to a receptor on a target cell, the antibody inhibits the signaling pathway, leading to decreased cell proliferation, increased secretion of pro-apoptotic factors, and / or cell death (Suzuki, Kato, and Kato 2015). Accordingly, a rise in demand for additional mAb therapies has necessitated an increase in mAb manufacturing capacity.

Protein therapeutics are typically delivered directly to the bloodstream, often to an immunocompromised patient. The FDA (and corresponding international regulatory agencies) has provided safety guidelines for the manufacturing of biological products to avoid potential adverse effects of bacterial or viral contamination (FDA 1998). This includes mandated steps for virus removal and / or inactivation, typically performed towards the end of the manufacturing process to ensure that there are no viruses or virus-like particles present in the final mAb product. Common virus inactivation techniques used for mAbs include a low pH hold. Other chemical inactivation steps and high temperature may lead to degradation of these products. Most current mAb manufacturing processes include a size-based membrane separation technique to ensure high levels of virus removal from the product stream without damaging the mAb.

Virus filtration has become a critical component in the overall viral clearance strategy for the production of both plasma-derived products, e.g., intravenous IgG (Burnouf and Radosevich 2003), and recombinant proteins produced from mammalian cell lines, e.g., monoclonal antibodies (Rayfield et al. 2015). Virus filters have been commercialized for the removal of both retrovirus (size > 50 nm) and parvovirus (size >20 nm), although most current processes use parvovirus filters since these provide effective size-based removal of all viruses.

In addition to their importance in bioprocessing, virus filters are some of the most selective membranes currently available commercially. Typical parvovirus filters have been shown to provide as much as 6-log removal (retention) of small parvovirus (Lute et al. 2007) while recovering more than 95% of the therapeutic protein in the permeate (Wickramasinghe et al. 2010). This is true even for monoclonal antibody (mAb) products that are approximately 12 nm in diameter (Baek, Singh, Arunkumar, and Zydney 2017), with some investigators reporting effective mAb diameters (as determined by dynamic light scattering) of more than 18 nm (Rayfield et al. 2015). Thus, these membranes have a selectivity (defined as the ratio of the transmission of the product to that of the virus) of nearly 10^6 for species that differ in size by considerably less than a factor of two. In contrast, the best reverse osmosis membranes have selectivities between water and Na^+ of less than 10^3 even though the radius of a hydrated sodium ion (0.72 nm) is nearly 3 times the radius of a water molecule (0.275 nm).

1.2 Previous studies of mAb transmission in virus filters

The high product recovery in virus filtration is somewhat surprising since available hydrodynamic models predict that a membrane with perfectly uniform cylindrical pores would have an actual sieving coefficient (S_a) well described by Equation (1) (L. Zeman and Wales 1981):

$$S_a = \left(1 - \frac{a}{r_p}\right)^2 \left[2 - \left(1 - \frac{a}{r_p}\right)^2\right] exp\left(-\frac{0.7146a^2}{r_p^2}\right) \quad (1\text{-}1)$$

where S_a is equal to the ratio of the protein concentration in the permeate to that in the solution immediately upstream of the membrane. For a parvovirus filter with r_p = 20 nm, the sieving coefficient for a 12 nm antibody given by Equation (1) is S_a = 0.23, which is well below the 95% or higher recovery observed in most virus filtration studies.

There have been relatively few direct studies of the transmission characteristics of virus filtration membranes. Wickramasinghe et al. (2010) reported bovine serum albumin (BSA) transmission through the Ultipor® DV20 filter as >98%, although this was the observed transmission without any effort to account for the effects of concentration polarization. Bakhshayeshi and Zydney (2008) evaluated the transmission of BSA through the Viresolve® 180 membrane as a function of membrane orientation and solution pH. Nearly 100% yield was obtained when the membrane was used with the selective skin-side down. However, the BSA yield (transmission) was significantly reduced when the membrane was oriented with the skin-side up, particularly at lower pH. This difference in behavior was assumed to be due to concentration polarization within the support structure when the membrane was used with the skin-side down. Similar results were obtained for retention of high molecular weight dextrans through the Viresolve® Pro, another highly asymmetric virus filter (Bakhshayeshi et al. 2011). The actual sieving coefficient for BSA through the Viresolve® 180 was estimated using available polarization models as being <1%, although this value was very sensitive to the empirical correlation used to evaluate the bulk mass transfer coefficient in the stirred cell (Bakhshayeshi and Zydney 2008). In addition, it is unclear how to extrapolate from data for BSA (approximately 7 nm in size) to the behavior of a monoclonal antibody.

1.3 Previous studies of filtration performance of virus filters

One challenge to overcome during virus filtration is membrane fouling. Since the feed at this point in the process is highly purified, the main foulant is primarily the protein product, or a subspecies of the product, such as aggregates or fragments (Bolton et al. 2005). Fouling is a complicated process, which involves protein-membrane interactions which cause adsorption to the membrane surface or within the pores. It is desirable to increase the filter capacity, or the maximum amount of product that can be processed per membrane area. Understanding the many factors that influence filter capacity is necessary for selecting the best membrane for the product and getting the most out of that filter by altering protein solution conditions.

In addition to the pore size, one of the key factors effecting virus filtration performance is the chemistry of the membrane polymer. Marques et al. performed experiments with virus filters with three different chemistries, polyethersulfone (PES), polyvinylidene fluoride (PVDF) and regenerated cellulose (RC). Their results suggested a correlation between improved filter performance and higher hydrophilicity due to minimization of nonspecific interactions between the membrane and the hydrophobic domains of the mAbs (Marques, Roush, and Göklen 2009).

Another import factor governing virus filter performance is the morphology of these membranes. Virus filters can have a homogenous (relatively uniform) pore size distribution throughout the depth of the filter, or they can have an asymmetric structure in which the pore size varies significantly through the filter. Syedain et al. studied the performance of asymmetric virus filtration membranes and found that orientation of the filter greatly affected performance. Asymmetric ultrafiltration membranes are almost always operated in tangential flow filtration systems with the selective skin layer facing the feed stream. Early virus filters were operated in a similar fashion. Syedain et al. found that with the skin-up, osmotic pressure affects drove the decrease in flux, while the osmotic pressure had little effect on the flux in the skin-down

orientation leading to an increase in membrane capacity. This indicates a different fouling mechanism was present even with the same membrane based on differences in orientation (Syedain, Bohonak, and Zydney 2006).

While membrane chemistry and morphology are certainly important factors governing the flux, the feed solution conditions and the properties of the antibody are also critically important. For example, studies done by Kosiol et al. using intravenous Immunoglobulin G (IVIG) found that re-filtering the feed through the same virus filter decreased the extent of flux decline, demonstrating that the virus filter is removing some species in the feed that is involved in membrane fouling. Further analysis by hydrophobic interaction chromatography showed that the more hydrophobic fractions of the feed fouled the membrane more extensively and also had larger z-average diameter as determined by dynamic light scattering (Kosiol et al. 2018). On the other hand, Bieberbach et al. examined the filtration performance of monoclonal antibodies obtained from mammalian cell cultures as purified process intermediates. They found that prefiltration of one of the mAbs through an adsorptive prefilter decreased the flux decline and the degree of fouling became nearly independent of the mAb concentration, suggesting that hydrophobic protein aggregates were the primary cause of the flux decline. On the other hand, pre-filtration had no effect on the flux behavior for a different mAb, and the flux remained highly dependent on the mAb concentration. Based on these results Bieberbach et al. concluded that this mAb displayed a reversible self-association that was concentration dependent and unaffected by pre-filtration. Further support for this conclusion was provided by the high negative interaction parameter for this mAb, indicating the presence of strong attractive forces between mAbs (Bieberbach et al. 2019).

Hongo-Hirasaki et al. conducted experiments with IgG and saw that increasing salt concentration, or ionic strength, caused an increase in the concentration of dimers leading to a decrease in the filter capacity. It is known that hydrophobic interactions are more important at

high salt concentrations, suggesting that dimer formation is enhanced by intermolecular hydrophobic interactions. They also found that increasing the IgG concentration caused an increase in the ratio of dimers to monomers, although there did not appear to be a strong correlation between flux decline and dimer content (Hongo-Hirasaki, Komuro, and Ide 2010).

1.4 Research Overview

The overall objective of this thesis is to determine the antibody retention by virus retentive filters and study the flux decline during filtration and investigate the mechanisms driving this decline.

Chapter 2 details the materials and methods used in this experiment. Specific details on the mAbs used in this study, as well as characteristics of the membranes are provided. The filtration experimental setups are explained as well as the antibody solution characterization techniques.

Chapter 3 discusses the antibody retention during filtration by virus filters. Virus filters are operated as normal flow filtration, which creates a high degree of polarization at the selective layer. By measuring the osmotic pressure of the antibody and operating in the low flux regime, a quantitative analysis of the antibody retention is presented.

Chapter 4 presents an investigation into the flux decline mechanisms of antibodies during filtration through virus filters. The role of pre-filters in virus filtration was explored to better explain the role of asymmetry in virus filters.

Chapter 5 summarizes the contributions of this work to the understanding of antibody flux through virus filters. Recommendations are provided for further study of antibody filtration.

Chapter 2

Materials and Methods

2.1 Monoclonal Antibody Solution

Several highly purified monoclonal antibody (mAb) products (post-Protein A with <1% high molecular weight species) were produced in Chinese Hamster Ovary (CHO) cells at Bristol Myers Squibb (Devens, MA) and provided as small (10 mL) frozen aliquots. The frozen samples were stored in a -80 °C freezer until use. A single aliquot was slowly thawed at 4 °C and then filtered through a 0.2 μm nominal pore size polyethersulfone syringe filter (VWR) to remove any insoluble aggregates that might have been generated during the freeze-thaw cycle. The mAb concentrations were adjusted by dilution with their respective buffers as summarized in Table **2-1**.

Table **2-1**: Solution properties of mAbs used in this work.

Antibody	Stock Conc. (g/L)	pI	Buffer Conditions
mAb-5	20.5	6.9	40 mM sodium phosphate, pH 6.0
mAb-4	23.7	7.9	40 mM citrate-phosphate, 100 mM NaCl, pH 5.5
mAb-10	23.6	8.6	40 mM sodium acetate, pH 5.5

2.2 Filters

2.2.1 Millipore Viresolve® Pro

The Viresolve® Pro virus filter has a highly asymmetric pore size through the depth of the 140 μm thick filter. The majority of the membrane is a porous support layer with the tight selective (skin) layer having a mean pore size around 20 nm (Fallahianbijan et al. 2017; Nazem-Bokaee et al. 2018). Figure **2-1** shows an SEM image through the cross-section of a Viresolve® Pro membrane.

Commercial virus filtration cartridges use two layers of the Viresolve® Pro in series to provide the high level of virus retention required in bioprocessing applications. The experiments conducted in this work used a single layer of membrane cut from a roll-stock sheet generously provided by MilliporeSigma (Bedford, MA). The Viresolve® Pro is normally operated with the skin layer facing downstream (away from the feed), with the porous support acting as a depth prefilter that protects the skin from deposition of any large particles or aggregates. In this work, this is referred to as "normal" orientation, whereas "reverse" orientation of the membrane is with the skin layer facing upstream (towards the feed).

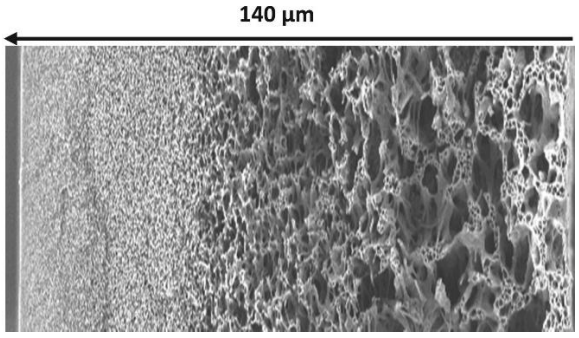

Figure **2-1**: SEM image of Viresolve Pro cross section, where skin is on left side of figure. Typical flow direction is from right to left (image reproduced from Fallahianbijan et al. 2017) with permission.

2.2.2 Pall Pegasus™ SV4

The Pegasus™ SV4 has a much more symmetric (uniform) pore size throughout the depth of the virus filter (David et al. 2019). This polyvinylidinedifluoride (PVDF) membrane has a nominal pore size of approximately 20 nm based on the ability to effectively retain very small parvovirus. Experiments were conducted with small disks cut from flat sheet membranes generously provided by Pall Corporation (Port Washington, NY).

2.2.3 Prefilters

The effect of different pre-filters with varying pore size, chemistry, and pore morphology on the performance of the virus filters were examined using several different flow configurations as discussed subsequently. The specifics of the different filters are detailed in Table **2-2**. The prefilters were placed upstream of the virus filters, such that the feed passed through these larger pore size filters prior to entering the virus filter.

Table **2-2**: Summary of properties of the prefilters used in this work.

Prefilter	Pore size (µm)	Chemistry	Porosity (%)
Durapore (Millipore)	0.1 – 5	PVDF	70
Magna™ (GVS)	5	Nylon	70-80
Isopore (Millipore)	5	Polycarbonate	5-20
Nylon Net (Millipore)	180	Nylon	47

2.3 mAb Filtration Experiments

The apparatus for running a filtration experiment consists of a pressurized reservoir connected to the lab air. A pressure regulator controls the pressure of air in the reservoir, which is

monitored during the experiment by observing the pressure gauge on the reservoir. At the bottom of the reservoir the solution flows through a valve into the membrane holder. The entire feed volume is collected from the outlet of the holder in sample tubes to measure flux and concentration during the filtration. A diagram of the experimental setup is shown in Figure **2-2**.

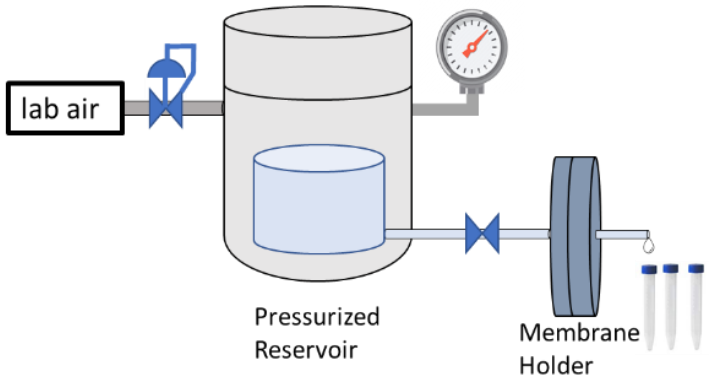

Figure **2-2**: Diagram of apparatus for filtration experiments.

All filtration experiments were conducted as follows. The virus filter was first cut from the larger flat sheet to fit the size of the filter holder (either 47 or 25 mm diameter) and placed directly on top of a 5 µm nylon support filter at the base of the holder to minimize deformation of the membrane into the support. The small disk was gently rinsed with deionized (DI) water to remove any dust or other large contaminants. The holder was assembled and sealed and the filter was flushed with DI water using a minimum volume of 40 L/m^2 (at the same transmembrane pressure to be used for the antibody filtration). The filter was then flushed with 20 L/m^2 of the buffer in which the mAb was formulated. Then the mAb solution was filtered through the holder for a specified volume. At the end of the filtration experiment, the system was emptied, refilled with buffer, and approximately 30 L/m^2 of buffer was flushed through the membrane to examine the reversibility of any fouling. Samples were taken during the initial buffer flush, mAb filtration,

and final buffer flush to evaluate the filtrate flux (by timed collection). The permeability of the membranes were evaluated from the ratio of the measured filtrate flux to the applied transmembrane pressure based on data obtained during the buffer flush. The normalized flux during the antibody filtration was defined as the filtrate flux obtained with the antibody divided by the buffer flux evaluated under the same conditions immediately prior to the antibody filtration.

2.3.1 Stainless steel holder

Some filtration experiments were performed in a 47 mm diameter stainless steel holder (MilliporeSigma, Bedford MA), which seals the membranes within by bolting the two halves together. A metal screen supports the membrane, then an O-ring is places on top before the two halves are bolted together. The bolts are tightened gradually moving around the holder, to not pinch the O-ring or damage the membrane. This holder is shown in Figure **2-3**, panel a).

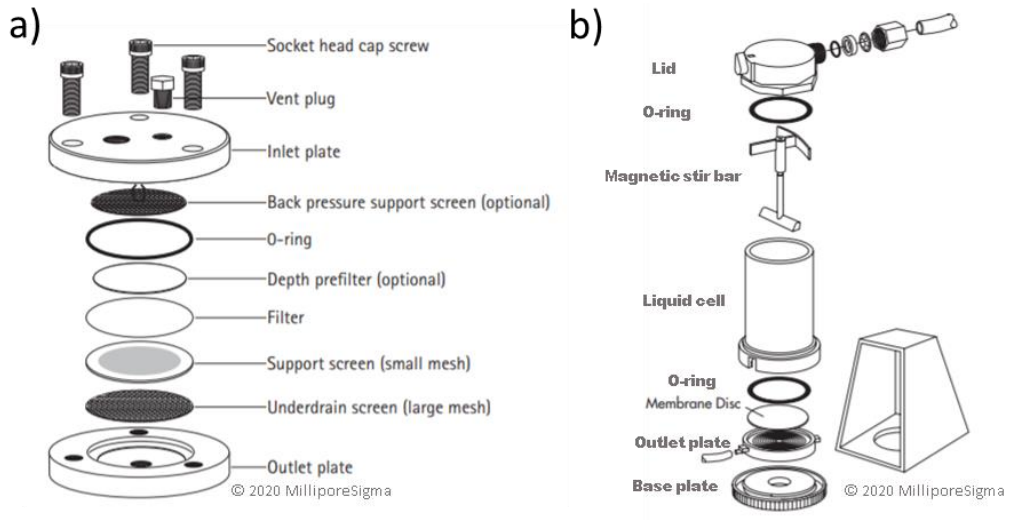

Figure **2-3**: Assembly diagrams for a) 47 mm stainless steel holder and b) Amicon 8000 series stirred cell.

2.3.2 Stirred cell holder

Protein filtration experiments were also performed in a Amicon® Model 8010 stirred cell (MilliporeSigma), which houses 25 mm diameter filters and holds 10 mL of solution above the membranes. This holder was fitted with a stir bar suspended from the top of the cell so that the stirrer was located just above the membrane. Data were obtained both with and without stirring (at a stir rate of 800 rpm). A diagram of the holder is shown in Figure **2-3**, panel b).

2.3.3 mAb prefiltration

Two different configurations were used for the prefiltration experiments. One is described as an "integral" prefilter, in which the prefilter is placed directly on-top of the virus filter within the same holder. The second is referred to as in-line prefiltration, where the prefilter and virus filter are housed in separate holders. The filtrate that passes through the pre-filter is fed directly into the downstream holder containing the virus filter.

2.4 Characterization Techniques

2.4.1 Absorbance

mAb concentrations were evaluated from the intrinsic absorbance at 280 nm using a Tecan Infinite 200 PRO spectrophotometer. Absorbance was measured in triplicate using 250 µL samples in a Greiner 96-well plate, with the mAb concentration calculated from the mean absorbance using a calibration curve prepared using solutions with known concentration.

2.4.2 Dynamic Light Scattering (DLS)

The mAb diffusivity was evaluated using a Malvern Zetasizer ZS90. A 60 μL sample was added to a quartz cuvette and loaded into the Zetasizer. The system was allowed to equilibrate for 2 minutes, at which point the light scattering intensity was measured for 10 seconds for several repeat runs. This procedure was repeated 3 times per sample to obtain the mean value of the mAb diffusion coefficient at the specific mAb concentration.

2.4.3 Size Exclusion Chromatography (SEC)

The presence of higher order aggregates in the mAb solutions was investigated using an Agilent 1260 Infinity II HPLC system (Agilent Technologies, Santa Clara, CA) with ultraviolet (UV) and refractive index (RI) detectors. A GE Superdex 200 column was used with a running buffer of 25 mM sodium phosphate and 300 mM L-arginine monohydrochloride at pH 7.8. The flow rate was 0.45 mL/min

2.4.4 Analytical Hydrophobic Interaction Chromatography (HIC)

Analytical HIC was used to evaluate the surface hydrophobicity of the different mAbs based on the approach described by Doss et al. (2019). A TSKgel Butyl-NPR Resin (TOSOH Bioscience) was used in a 4.6 mm x 10 cm column in a Thermo Scientific Vanquish UHPLC with a variable wavelength UV-Vis detector. The column was initially equilibrated with a buffer containing 0.1 M sodium phosphate and 2.3 M ammonium sulfate at pH 7.0. Then the sample was injected and able to bind to the resin in the presence of the high ammonium sulfate concentration. A gradient elution was performed, with the ratio of phosphate to ammonium sulfate increased from 0% to 100% over 70 minutes at a flow rate of 0.35 mL/min.

2.4.5 Capillary viscometry

Capillary viscometry was used to measure the viscosity of the mAb solution. Data were obtained with a Masterflex PVC capillary tubing of length L = 7.5cm and radius r = 0.0095 cm, with the volumetric flow rate (q) measured as a function of the pressure (ΔP) which was set by adjusting the height of solution in a small reservoir positioned above the horizontal capillary. The viscosity was evaluated using the Hagen-Poiseuille equation:

$$q = \frac{\pi r^4 \Delta P}{8 \mu L} \qquad (2-1)$$

Data were also obtained in the same capillary using the buffer, with the relative viscosity evaluated from the ratio of the viscosity of the antibody solution to that of the protein-free buffer.

2.4.6 Osmotic Pressure

The osmotic pressure of the mAb was evaluated in the stirred cell following the procedures described by Binabaji et al. (Binabaji, Rao, and Zydney 2014). In this case, the stirred cell was fitted with a 30 kDa Biomax® membrane (MilliporeSigma) that was fully retentive to the mAb. The mAb was concentrated 5-fold to approximately 100 g/L using an applied pressure of 210 kPa. The pressure was then reduced to <14 kPa and the filtration continued until the flux became essentially zero as determined by the cessation of motion of the meniscus in a small diameter piece of tubing connected to the filtrate exit port. The stirred cell was then opened and a small sample obtained to evaluate the mAb concentration. The osmotic pressure of the mAb solution at that concentration is equal to the applied pressure at which the filtrate flux became zero. The stirred cell was then sealed, the pressure increased slightly, and the entire procedure repeated to evaluate the osmotic pressure over a range of mAb concentrations.

Chapter 3

Antibody retention by virus filtration membranes: polarization and sieving effects

The work presented in this chapter is adapted from: **M. Billups**, M. Minervini, M. Holstein, H. Feroz, S. Ranjan, J. Hung, H. Bao, S. Ghose, Z.J. Li, A.L. Zydney, Antibody retention by virus filtration membranes: Polarization and sieving effects, J. Memb. Sci. 620 (2021) 118884. https://doi.org/10.1016/j.memsci.2020.118884.

3.1 Concentration Polarization Effects

Figure **3-1** shows experimental data for the observed sieving coefficient (top panel) and filtrate flux (bottom panel) for filtration of a 3.9 g/L solution of the mAb through a Viresolve® Pro membrane oriented with the selective skin layer facing up. The skin-up orientation was used to provide better control over the concentration polarization boundary layer (instead of having the polarization occur within the porous support of the Viresolve® Pro). Data were obtained at a constant transmembrane pressure of 5.1 kPa (0.7 psi). The initial data point at a filtrate flux of 21 $L/m^2/h$ (LMH), equal to 5.8 μm/s, is the value obtained with the phosphate buffer (at the same pressure) immediately prior to filling the stirred cell with the antibody solution. The experiment consisted of three distinct phases: the first and third were stirred at approximately 800 rpm, while the stirrer was turned off at the start of the second phase. The stirred cell was kept sealed with the membrane in place throughout the entire filtration, without any disruption in the applied pressure. The results are plotted as a function of the volumetric throughput, defined as the cumulative volume of filtrate processed divided by the membrane area.

The filtrate flux during the stirred filtration phase immediately decreased to 15 LMH (4.2 µm/s) and remained relatively stable throughout the first phase. There was a sharp decrease in flux as soon as the stirring was turned off in the second phase, with the flux decaying over a period of approximately 40 min (corresponding to 4 L/m^2 of filtration) to a final value of 5.0 LMH (1.4 µm/s), which is less than 25% of the initial buffer flux. Restarting the stirrer caused an immediate increase in the filtrate flux, attaining a value that was just slightly smaller than the flux measured during the first phase of the filtration. This suggests that the decline in flux seen during the second (unstirred) phase is entirely reversible, consistent with the effects of concentration polarization. This is discussed in more detail subsequently.

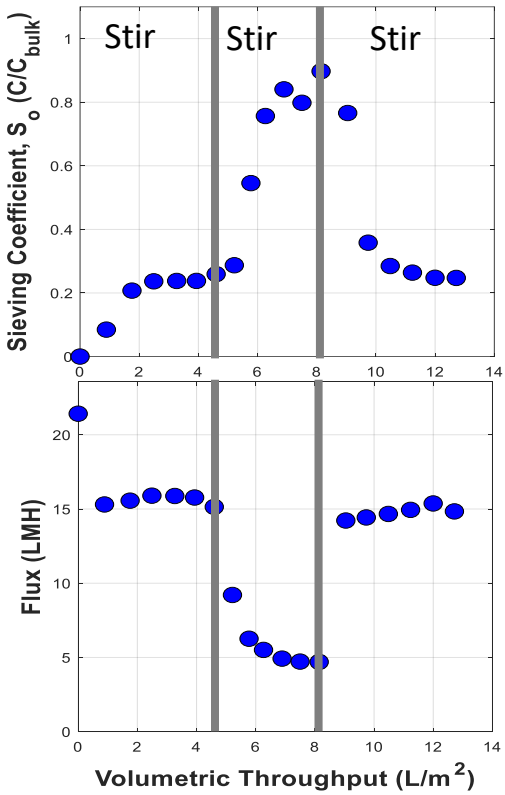

Figure **3-1**: Observed sieving coefficient (top panel) and filtrate flux (bottom panel) during filtration of a 3.9 g/L mAb solution through the Viresolve® Pro membrane with the skin-side up (facing the feed) at a pressure of 5.1 kPa. Data were obtained in 3 phases: stirred, unstirred, and then stirred (at a stirring speed of 800 rpm).

The top panel in Figure **3-1** shows the corresponding data for the observed sieving coefficient, defined as the ratio of the antibody concentration in the permeate samples (C) divided by the initial concentration of the antibody feed loaded into the stirred cell (C_{bulk}). The observed sieving coefficient increased over the first 2 L/m^2 (corresponding to a filtrate volume of 0.72 mL), reflecting the washout of the phosphate buffer from the region beneath (downstream) of the Viresolve® Pro membrane in the stirred cell. The observed sieving coefficient then approached a nearly constant value of 0.24, clearly indicating that the Viresolve® Pro has significant retention of the antibody. The observed sieving coefficient increased rapidly in Phase 2 due to the increase in the antibody concentration in the solution immediately upstream of the membrane surface arising from the reduction in back mass transfer when the stirrer is turned off. This effect was completely reversible, with S_o decreasing back to a value of 0.25 when the stirrer was turned back on. The slightly higher value of the observed sieving coefficient in Phase 3 compared to that in Phase 1 was due to the accumulation of retained antibody in the stirred cell over the course of the filtration. The final antibody concentration in a sample obtained directly from the stirred cell at the end of the experiment was 4.3 g/L, which is approximately 10% higher than the initial concentration.

The effect of concentration polarization on the observed sieving coefficient in the stirred cell can be quantified using the classical stagnant film model (Blatt et al. 1970):

$$S_o = \frac{C}{C_b} = \frac{S_a}{(1 - S_a)\exp\left(-\frac{J_v}{k_m}\right) + S_a} \qquad (3-1)$$

where J_v is the filtrate flux and k_m is the mass transfer coefficient in the stirred cell. The actual sieving coefficient is defined as $S_a = C/C_w$, where C_w is the mAb concentration immediately adjacent to the upstream surface of the membrane (often referred to as the "wall" concentration).

A common approach for evaluating S_a and k_m is to rearrange Equation (3-1) in the following linearized form as (Hadidi, Buckley, and Zydney 2015):

$$\ln\left(\frac{1}{S_o}-1\right)=\ln\left(\frac{1}{S_a}-1\right)-\frac{J_v}{k_m} \qquad (3-2)$$

with the slope equal to $1/k_m$ and the intercept directly related to S_a. Experimental data for the observed sieving coefficient from a series of filtration experiments performed at different applied pressures and bulk concentrations, all using the Viresolve® Pro oriented with the skin-side up in the stirred system, are plotted in Figure **3-2** in the form given by Equation (3-2). The observed sieving coefficients range from 0.05 (for the 20 g/L solution at a pressure of 14 kPa) to a value of $S_o = 0.47$ (for the 4 g/L solution at a pressure of 10 kPa). Although the data show a clear decrease in the sieving function with increasing filtrate flux, consistent with Equations (3-1) and (3-2), the results show significant curvature with an R^2 value of only 0.73, in sharp contrast to data obtained in other studies, e.g., polysaccharide filtration through ultrafiltration membranes. This makes it very difficult, if not impossible, to evaluate either the actual coefficient or the bulk mass transfer coefficient using this linearized form of the concentration polarization model. Instead, the curvature observed in Figure **3-2** suggests that the actual sieving coefficient and / or the mass transfer coefficient in Equation (3-2) do not remain constant over the range of bulk concentrations and filtrate flux examined in these experiments. The origin of this behavior, and an alternative approach for evaluating S_a and k_m, are presented in the next section.

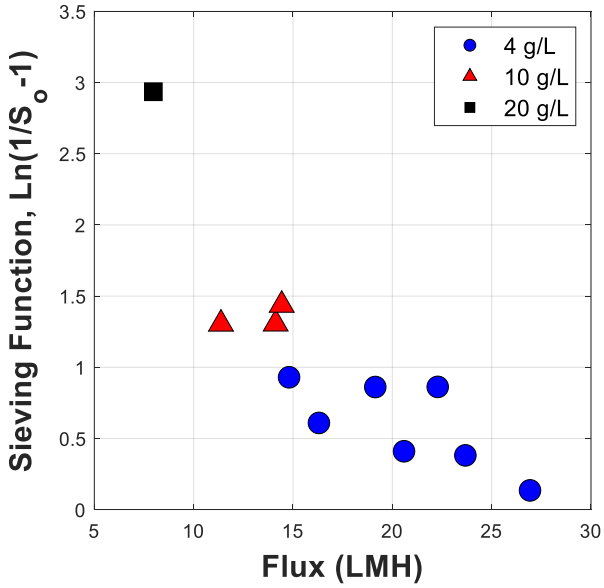

Figure **3-2**: Observed sieving coefficient data obtained over a range of applied pressures and antibody concentrations plotted in the linearized form given by Equation (3). Data were obtained in the presence of stirring at 800 rpm.

3.2 Osmotic Pressure Analysis

An alternative approach for evaluating the effects of concentration polarization on the filtration behavior is from the dependence of the filtrate flux on the effective pressure driving force, defined as the difference between the applied transmembrane pressure (ΔP) and the osmotic pressure of the concentrated antibody solution at the upstream surface of the membrane (ΔΠ) (Deen 1987):

$$J_v = L_p(\Delta P - \sigma_0 \Delta \Pi) \qquad (3-3)$$

where L_p is the membrane hydraulic permeability and σ_o is the Staverman (osmotic) reflection coefficient (Kedem and Katchalsky 1958). Equation (3-3) can be rearranged to evaluate the osmotic pressure from the measured values of the filtrate flux assuming that the membrane

hydraulic permeability in the presence of the antibody solution is the same as that evaluated with the buffer; this is discussed in more detail subsequently. The data in Figure **3-1** give an osmotic pressure of 1.0 kPa using the filtrate flux evaluated during the first phase of the experiment based on σ_o = 1 and L_p = 1.2 μm/s/kPa (29 L/m^2/h/psi), with the latter determined for the clean membrane using the protein-free phosphate buffer. The effect of the osmotic reflection coefficient on the calculations are discussed in more detail subsequently.

Independent measurements of the osmotic pressure of the antibody solution as a function of the mAb concentration were obtained as described in Section 2.4.6. The experiments were performed in the stirred cell using a fully retentive Biomax® 30 kDa membrane (σ_o = 1). The stirred cell was pressurized to a pre-set value, with the osmotic pressure determined from Equation (3-3) at the point where the flux was equal to zero as determined by the cessation of motion of the meniscus in a narrow bore tubing on the permeate exit. The tubing was observed for a minimum of 30 min without any noticeable movement of the meniscus, which corresponds to a filtrate flux of J_v < 0.07 μm/s (<0.25 LMH) based on the inner diameter of the narrow bore tubing. Thus, the osmotic pressure could be evaluated to an accuracy of better than 0.066 kPa based on the measured membrane permeability, where the maximum error in the calculated value of ΔP is simply $J_{v,max}/L_p$.

The osmotic pressure of the mAb solution increased from 3.3 kPa at a concentration of 130 g/L to more than 13 kPa at an antibody concentration of 260 g/L (Figure **3-3**). The value at 13 kPa was determined twice with separate mAb solutions, with the measured antibody concentrations at this osmotic pressure differing by less than 0.4%. These osmotic pressure values are similar in magnitude to previous data for other mAbs evaluated under similar buffer conditions (Baek, Singh, Arunkumar, Borys, et al. 2017). The data in Figure **3-3** were fit to a 3rd order virial expansion (Vilker, Colton, and Smith 1981):

$$\Pi = \left(\frac{k_B T N_A}{10^3 M_P}\right) C \quad + B_2' C^2 \; + B_3' C^3 \qquad (3-4)$$

where k_B is Boltzmann's constant, T is the absolute temperature, N_A is Avogadro's number, M_P is the molecular weight of the antibody, and C is the antibody concentration (in g/L). The virial coefficients were evaluated in Matlab using a least-squares fit giving $B_2' = 6.7 * 10^{-5}$ kPa L^2/g^2 and $B_3' = 7.0 * 10^{-7}$ kPa L^3/g^3.

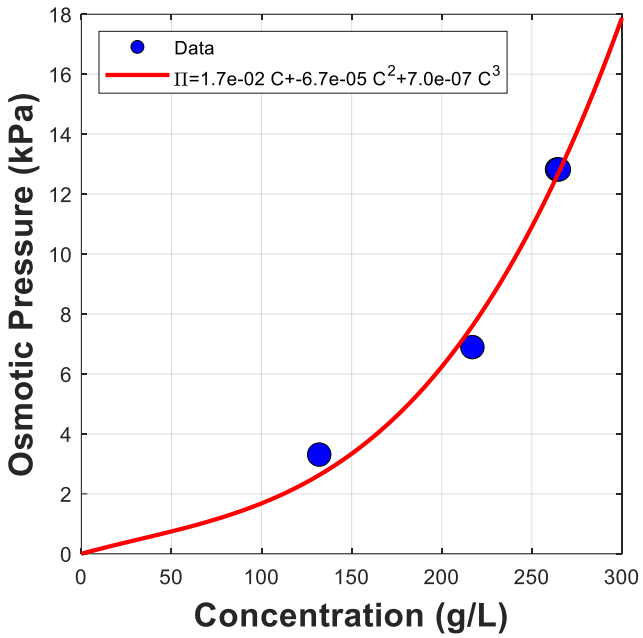

Figure **3-3:** Osmotic pressure as a function of the antibody concentration. Solid curve is a fit to the data determined using a 3rd order virial expansion.

The actual sieving coefficients for each experiment with the Viresolve® Pro membrane were evaluated as follows. First, the osmotic pressure was calculated by rearranging Equation (3-3) as:

$$\Delta\Pi = \Delta P\left(1 - \frac{J_v}{J_o}\right) \qquad (3-5)$$

where J_v and J_o are the filtrate flux with the antibody solution and with the phosphate buffer, respectively, both at the same ΔP. Note that Equation (3-5) assumes that $\sigma_o \approx 1$; calculations performed using osmotic reflection coefficients as small as 0.9 caused less than a 10% shift in the actual sieving coefficient. The calculated values of the osmotic pressure were then used to evaluate the antibody concentration at the upstream surface of the membrane (C_{wall}) using Equation (3-4), with the actual sieving coefficient then evaluated from the measured filtrate concentration as:

$$S_a = \frac{C_{filtrate}}{C_{wall}} \qquad (3-6)$$

The results for the actual sieving coefficients for experiments performed at 4, 10, and 20 g/L bulk antibody concentrations are summarized in Figure **3-4**. The actual sieving coefficients determined using Equations (3-5) and (3-6) range from S_a = 0.004 at an antibody wall concentration of 260 g/L to slightly more than 0.05 at C_{wall} = 21 g/L. These results demonstrate that the Viresolve® Pro is highly retentive to the monoclonal antibody, with transmission well below 5% under most conditions. The decrease in the actual sieving coefficient with increasing wall concentration is discussed in more detail subsequently.

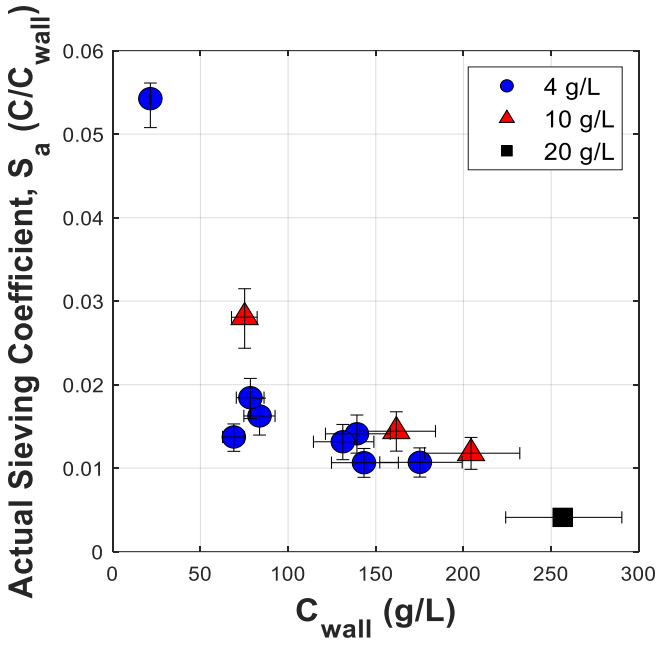

Figure **3-4**: The actual antibody sieving coefficient for the Viresolve® Pro membrane evaluated from the C_{wall} values determined from the osmotic pressure correlation.

One key assumption in the evaluation of the actual sieving coefficients in Figure **3-4** is that the permeability in the presence of the antibody is equal to that evaluated prior to the experiment with pure phosphate buffer. The very similar values for the filtrate flux in the first and third phases in Figure **3-1** do suggest that membrane fouling was negligible in these experiments. This was confirmed by measuring the buffer flux through the membrane at the end of the experiment by replacing the antibody solution in the stirred cell with the phosphate buffer. The buffer flux increased rapidly as residual antibody was washed out of the stirred cell, with the flux attaining a value that was within 5% of the original (clean) buffer flux within 10 L/m^2 of filtration.

In order to examine the effect of a low level of protein fouling on the calculated values of the actual sieving coefficient, the calculations were repeated assuming that the permeability in the presence of the antibody was 10% less than that determined with the phosphate buffer, i.e., L_p =

0.9 L_{po}. For the data in Figure **3-1**, this change in permeability caused the osmotic pressure to decrease from 1.05 to 0.63 kPa, leading to a 40% reduction in the calculated value of the antibody concentration at the wall (from 69 to 42 g/L). The net result is an increase in actual sieving coefficient from $S_a = 0.014$ to $S_a = 0.022$. Even smaller changes in S_a were seen for most of the other data, with overall dependence of the actual sieving coefficient on C_{wall} being very similar to that shown in Figure **3-4**.

The experimental data during the second phase of the filtration experiment in Figure **3-1** do show an observed sieving coefficient of nearly 90% towards the end of the unstirred period. If we assume that the actual sieving coefficient for this membrane is $S_a \approx 0.02$ based on the data in Figure **3-4**, then we can immediately evaluate the wall concentration in the absence of stirring as:

$$C_{wall} = \left(\frac{S_o}{S_a}\right) C_{bulk} \qquad (3-7)$$

giving $C_{wall} \approx 160$ g/L. The osmotic pressure at this wall concentration is 3.8 kPa, with the corresponding value of the filtrate flux given by Equation (3-3) of $J_v = 5.5$ LMH. This is in good agreement with the measured value of the filtrate flux during the unstirred portion of the filtration experiment. Thus, the transient increase in the observed sieving coefficient seen in the unstirred portion of the experiment in Figure **3-1**, and the corresponding decrease in the filtrate flux, were both due to the time required to build up this high value of the wall concentration when the stirrer was turned off.

3.3 Mass Transfer Coefficient

The calculated values of the wall concentration can be directly used to estimate the mass transfer coefficient for the antibody in the stirred cell by rewriting Equation (3-1) as:

$$k_m = J_v \left[\ln \left(\frac{C_{wall} - C_{filtrate}}{C_{bulk} - C_{filtrate}} \right) \right]^{-1} \qquad (3-8)$$

The calculated values of k_m corresponding to all of the data in Figure **3-4** are shown in Figure **3-5** as a function of the wall concentration determined from the osmotic pressure analysis. The mass transfer coefficients decrease with increasing C_{wall}, going from a value of 2.1 µm/s at a wall concentration of 20 g/L to slightly under 1.0 µm/s at a wall concentration of 260 g/L. The data also tend to cluster based on the bulk concentration, with the values at 4 g/L lying above those at 10 g/L which are in turn greater than the single value determined at a bulk concentration of 20 g/L.

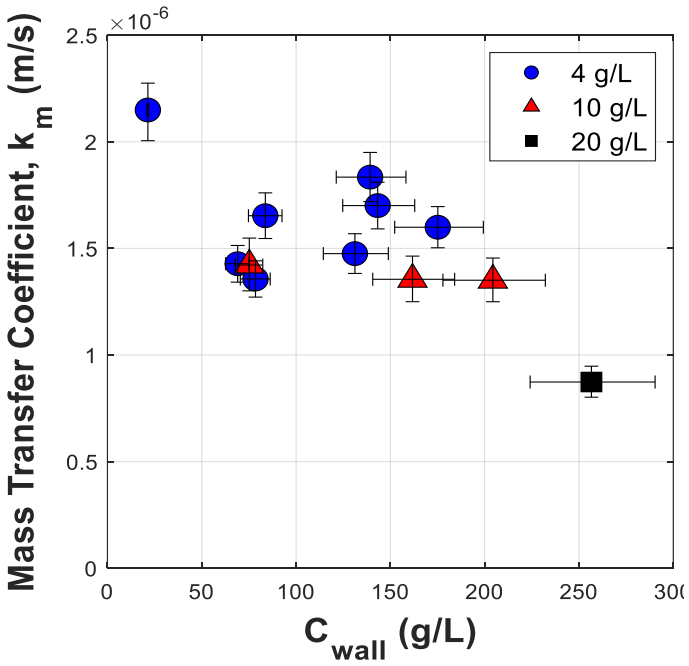

Figure **3-5:** Calculated values of the mass transfer coefficient as a function of the antibody concentration at the membrane surface. Error bars represent confidence intervals determined based on propagation of error analysis.

The values of the mass transfer coefficient given in Figure **3-5** can be compared with predictions from available literature correlations for mass transfer in a stirred cell (Opong and Zydney 1991):

$$k_m = \chi \left(\frac{\omega b^2}{\nu} \right)^{0.567} \left(\frac{\nu}{D} \right)^{0.33} \frac{D}{b} \qquad (3-9)$$

where ω is the stirring rate, ν is the kinematic viscosity, D is the protein diffusion coefficient, and b is the radius of the stirred cell. The coefficient χ is a function of the detailed device geometry and impeller location. Opong and Zydney (1991) evaluated χ = 0.23 based on filtrate flux data through fully-retentive ultrafiltration membranes in a similar stirred cell geometry. The antibody diffusion coefficient was measured using dynamic light scattering at different mAb concentrations, with results summarized in Figure **3-6**. The diffusion coefficient decreases nearly linearly with increasing mAb concentration, going from a value of 4.0 x 10^{-11} m^2/s for the 1 g/L solution to 1.8 x 10^{-11} m^2/s at a mAb concentration of 21 g/L. This reduction in diffusivity is consistent with the presence of strong intermolecular attractive interactions between the antibody molecules, which is likely due to self-association possibly driven by hydrophobic interactions(Bieberbach et al. 2019). The calculated values of the mass transfer coefficient given by Equation (3-9) range from 4.7 x 10^{-6} to 2.1 x 10^{-6} m/s using the high and low values of the mAb diffusion coefficient in Figure **3-6**. These values are about twice as large as those determined experimentally, which likely reflects the differences in the stirred cell geometry and the assumptions involved in evaluating the mass transfer coefficient based on Equation (3-8) using the estimated values of the wall concentration.

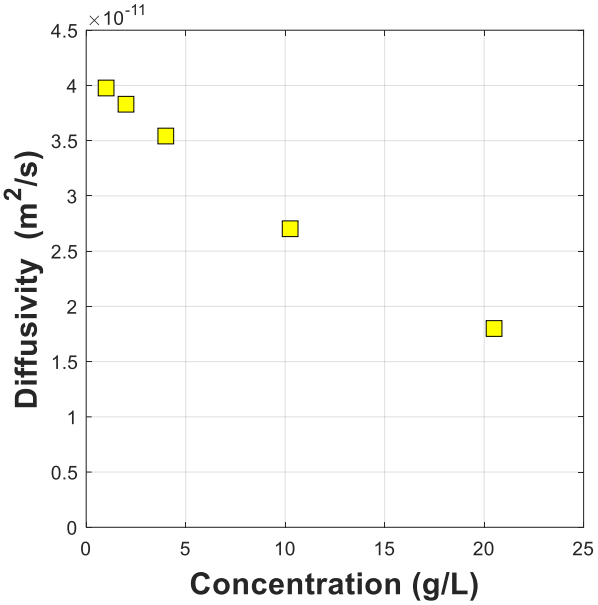

Figure **3-6:** Antibody diffusivity as a function of mAb concentration as determined by dynamic light scattering.

The correlation presented in Equation (3-9) indicates that the mass transfer coefficient should scale with $D^{2/3}$. The calculated mass transfer coefficients have been scaled by the measured diffusivity at the corresponding bulk concentration (D), with the resulting values plotted in Figure **3-7**, where D_∞ is the diffusivity at infinite dilution (determined by extrapolation of the data to C = 0). Although there is clearly considerable scatter in the data, the scaled mass transfer coefficients are nearly independent of the wall concentration; the calculated slope using a linear regression fit to the data was not statistically different than zero (slope = -0.002 ± 0.003 $\frac{\mu m/s}{g/L}$). These results provide further confirmation that the calculated values of the mass transfer coefficient determined from the measured values of the filtrate flux and protein osmotic pressure effectively describe the mass transfer characteristics of the antibody in the stirred cell system.

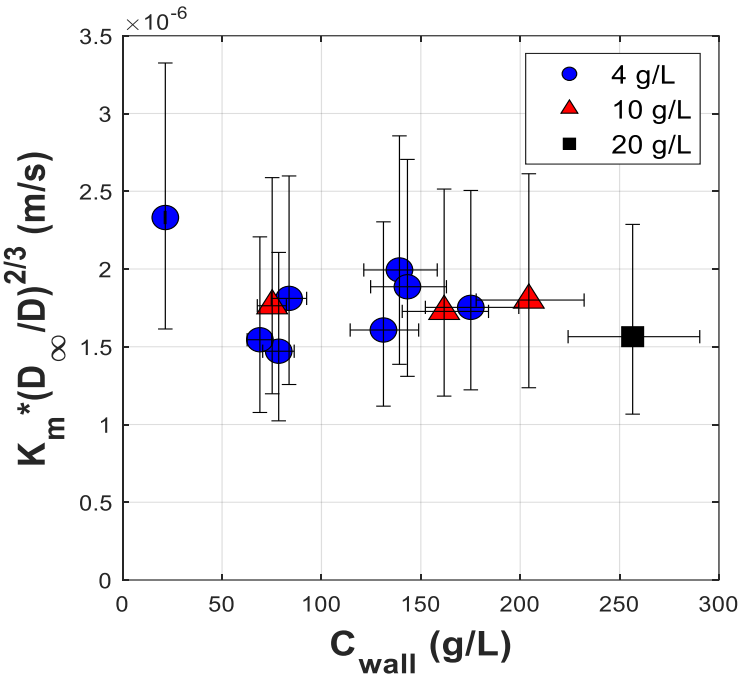

Figure **3-7**: Normalized mass transfer coefficient as a function of the wall concentration. Error bars show the 95% confidence interval determined by propagation of error analysis.

3.4. Pegasus SV4

Additional insights into mAb retention during virus filtration were obtained by performing a parallel set of experiments with the Pall Pegasus™ SV4, a polyvinylidene fluoride (PVDF) membrane with a relatively homogeneous pore size throughout the depth of the filter (Leisi et al. 2020). Since the SV4 has a much smaller hydraulic permeability than the Viresolve® Pro (by approximately 10-fold), data were obtained at higher pressures to give similar values of the filtrate flux for the two membranes. Typical data are shown in Figure 8 for the SV4 oriented with the shiny-side up (left panels). The general behavior is very similar to that seen previously for the Viresolve® Pro: the sieving coefficient initially increases as the hold-up volume is removed while the filtrate flux with the mAb is slightly less than that with buffer. Turning off the stirrer in Phase 2 caused an immediate reduction in the filtrate flux and a corresponding increase

in the observed sieving coefficient consistent due to the increase in concentration polarization. However, in contrast to the data with the Viresolve® Pro, the changes in flux and mAb transmission are not fully reversible; the observed sieving coefficient in Phase 3 is only 0.2, which is about one-half the value in Phase 1, and the filtrate flux in Phase 3 is also somewhat smaller than the value during the initial portion of the experiment. This is likely due at least in part to the increase in bulk concentration from 9.6 g/L at the start of the experiment to 11 g/L at the end of Phase 1 and then almost 13.3 g/L at the start of Phase 3.

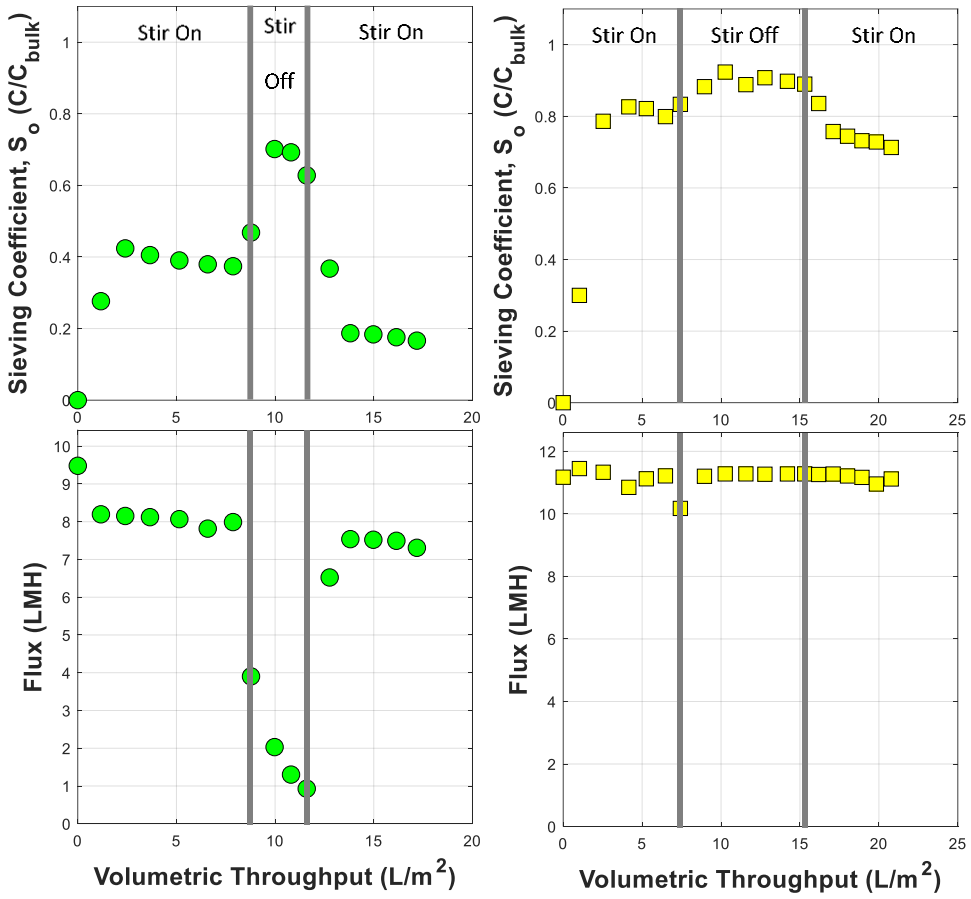

Figure **3-8**: Observed sieving coefficient (top panels) and filtrate flux (bottom panels) during filtration of a mAb solution (initial concentration of 9.6 g/L) through the SV4 membrane with the shiny-side up (facing the feed) at a pressure of 28 kPa (left panels) and a 4.5 g/L mAb solution through the SV4 membrane with shiny-side down (away from feed) at a pressure of 41 kPa (right panels). Data were obtained in 3 phases: stirred, unstirred, and then stirred (at a stirring speed of 800 rpm).

The data in Figure **3-8** were used to calculate the osmotic pressure (via Equation 3-5), the wall concentration (using Equation 3-4), the mass transfer coefficient (via Equation 3-8), and the actual sieving coefficient (via Equation 3-6), with results summarized in Table **3-1**, including data over a range of bulk concentrations and transmembrane pressures. The calculations were all performed using the data at the end of the first phase to ensure that the flux and observed sieving coefficient had stabilized. The actual sieving coefficients for the SV4 were all less than 0.05, with values that increase with decreasing wall concentration, in good qualitative agreement with the results for the Viresolve® Pro (Figure **3-4**). The similar values of the actual sieving coefficient for the SV4 and Viresolve® Pro are consistent with the similar virus retention characteristics of these filters, both of which are designed to retain 20 nm viruses. The calculated values of the mass transfer coefficients determined from the SV4 data range from 1.5 to 2.6 μm/s, which are also similar to the results obtained with the Viresolve® Pro (summarized in Figure **3-5**).

The last row in Table **3-1** (indicated by the asterisk) shows the results obtained with the SV4 oriented with the shiny-side down (from right hand panels in Figure **3-8**). The filtrate flux for this experiment was nearly independent of the stirring, with only a very small increase in the observed sieving coefficient when the stirrer was turned off. This suggests that the concentration polarization boundary layer with the shiny-side down is located primarily inside the porous structure of the SV4 (which is unaffected by stirring). In addition, the calculated value of the actual sieving coefficient for this orientation (S_a = 0.046) is considerably larger than the values obtained with the shiny-side up, suggesting that the SV4 has a measurable degree of asymmetry.

Table **3-1:** Summary of filtrate flux and sieving results for Pegasus^{TM} SV4 including calculated values of the osmotic pressure, wall concentration, mass transfer coefficient, and actual sieving coefficient. *Represents experiment with the shiny-side down (right panels in Figure **3-8**).

C_b (g/L)	ΔP (kPa)	J_v (LMH)	J_v/J_0	S_o	ΔΠ (kPa)	C_w (g/L)	k_m (μm/s)	S_a
11	55	15	0.70	0.26	16.5	290	2.6	0.0096
4.6	55	17	0.80	0.37	11.0	250	2.5	0.0067
4.3	55	17	0.87	0.56	6.9	210	2.4	0.012
11	28	8	0.84	0.38	4.4	170	1.6	0.025
4.0	41	13	0.94	0.45	2.5	130	2.0	0.014
4.5*	41	11	0.97	0.82	1.2	80	1.5	0.046

3.5. Actual Sieving Coefficients

Most previous studies of the concentration dependence of the actual sieving coefficient have reported an increase in S_a with increasing feed concentration. This includes data for bovine serum albumin and ficoll filtration through track-etch polycarbonate membranes (Mitchell and Deen 1986) as well as the transport of pegylated α-lactalbumin through composite regenerated cellulose membranes (Ruanjaikaen and Zydney 2013). In general, the actual sieving coefficient can be written as a function of the solute concentration as:

$$S_a = S_{a,o}\left[1 + \frac{\beta C}{\rho_p}\right] \qquad (3-10)$$

where $S_{a,o}$ is the actual sieving coefficient in the limit of an infinitely dilute solution, ρ_p is the protein density, and β describes the first-order correction to the actual sieving coefficient associated with intermolecular interactions. Theoretical analysis of the filtration behavior of purely hard-sphere solutes gives $\beta \approx 8.6$ (Adamski and Anderson 1983), which is very similar to the value predicted from the concentration dependence of the partition coefficient between the bulk solution and the membrane pores (which gives $\beta \approx 8.0$ as discussed by Zydney, 1992).

The diffusivity data in Figure **3-6** indicate that the mAb examined in this work has strongly attractive interactions, causing a sharp reduction in the diffusivity with increasing mAb concentration. The diffusion interaction parameter (k_D) can be evaluated by linear regression fit of the data:

$$D = D_\infty[1 + k_D C] \qquad (3-11)$$

giving k_D = -0.028 m^3/kg. As a first approximation, the coefficient β can be written in terms of the interaction parameter as (Zydney 1992):

$$\beta \approx 6.5 + \rho_p k_D \qquad (13-12)$$

which gives β = -30 using ρ_p = 1300 kg/m^3. This large negative value of β is in good qualitative agreement with the experimental results in Figure **3-4**. Note that a more accurate analysis of the concentration dependence of the actual sieving coefficient would require consideration of the effects of intermolecular interactions on bulk mass transfer in the concentration polarization boundary layer as discussed by Zydney (1992).

Previous studies of membrane sieving have suggested that the pore size distribution can be well approximated using a log-normal distribution:

$$n(r) = \frac{n_o}{r\sqrt{2\pi}}\left[ln\left(1 + \left(\sigma/\bar{r}\right)^2\right)\right]^{-\frac{1}{2}} exp\left\{-\frac{\left\{\ln\left\{\left(r/\bar{r}\right)\left[1+\left(\sigma/\bar{r}\right)^2\right]^{\frac{1}{2}}\right\}\right\}^2}{2ln\left[1+\left(\sigma/\bar{r}\right)^2\right]}\right\} \qquad (3\text{-}13)$$

where r is the pore radius, $\bar{r}$ is the mean pore size, and σ is the standard deviation. The actual sieving coefficient can be evaluated by integration over the pore size distribution (Mochizuki and Zydney 1993):

$$S_a = \frac{\int_0^\infty n(r) S_a(r) r^4 dr}{\int_0^\infty n(r) r^4 dr} \qquad (3-14)$$

where $S_a(r)$ is the actual sieving coefficient given by Equation (1-1). Mehta and Zydney (2005) showed that the permeability-selectivity tradeoff of currently available ultrafiltration membranes is well-described using the above equations with $\sigma/\bar{r} = 0.2$. Assuming that a single layer of the Viresolve® Pro provides LRV = 3 (i.e. $S_a = 0.001$) for a 20 nm virus, Equations (3-13) and (3-14) give $\bar{r}$ = 6.5 nm (with $\sigma/\bar{r} = 0.2$). The predicted sieving coefficient of a 12 nm diameter antibody through a membrane with this pore size distribution is $S_a = 0.078$, which is only slightly larger than the value obtained in the limit of very low antibody concentrations for the data in Figure **3-4**. These results suggest that the pore size distribution of the Viresolve® Pro is similar to (or just slightly tighter than) that of current state-of-the-art ultrafiltration membranes, with the very high selectivity arising largely from concentration polarization effects.

Chapter 4

Flux decline of during mAb filtration through virus filters

4.1 Filtration performance

To analyze the filtration performance, the filtrate flux and concentrations are measured. For the virus filtration process, the goal is to process all of the feed material as fast as possible, and with as little mAb loss as possible. Our goal in this work, rather than to outright maximize performance, is to understand what drives the filtration performance of mAbs through these virus retentive membranes.

To start, we first compared these mAbs at the concentrations provided to us by our industrial collaborators through both the Viresolve® Pro and the Pegasus™ SV4 virus filters operated as specified by the manufacturer (skin-side down). Figure **4-1** shows the normalized flux, or the filtrate flux of mAb solution divided by the flux of the initial buffer equilibration immediately prior to mAb filtration experiment, as a function of the volumetric throughput, or the volume of solution normalized by the membrane area. Presenting flux data in this way allows for accurate comparisons between experiments which have inherent variability in membrane permeability and the use of different sized holders. We can see in Figure **4-1** that all three of the mAbs have some similar flux behaviors through both virus filters. First is the rapid flux decline observed. On the normalized flux plot, every dataset starts at 1 because at the very start of the experiment, the flux is assumed to be the same as the buffer flush immediately prior. Then, by the first data point collected around 2 $\mathrm{L/m^2}$, the flux can drop as much as 95% and as little as 40%.

This behavior is markedly different from what classical filter fouling models (pore blockage, pore

constriction, cake formation) would predict; gradual decline in flux rather than this sharp decrease at the onset of mAb filtration like shown here (L. J. Zeman and Zydney 1996).

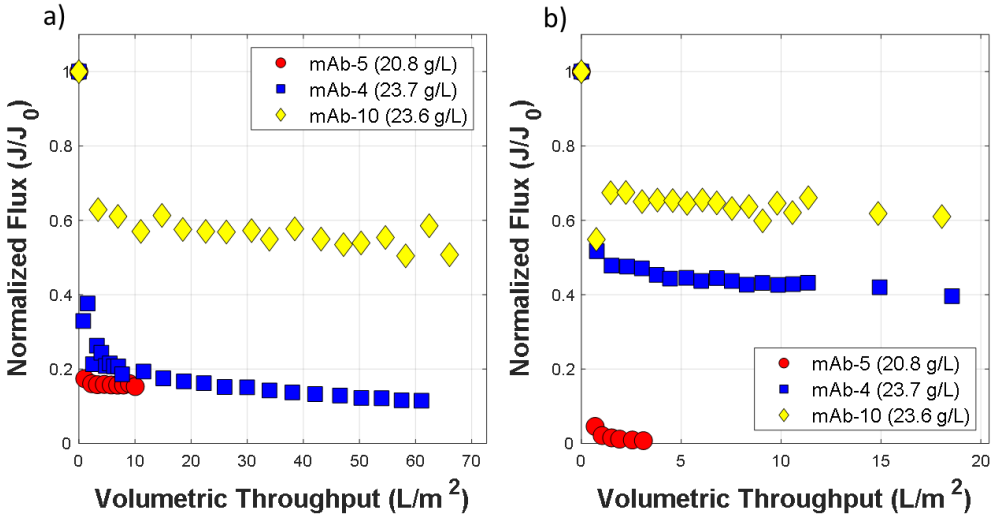

Figure **4-1**: The normalized flux vs volumetric throughput of the mAb solutions through the a) Viresolve® Pro and b) Pegasus™ SV4 membranes. All of these experiments were run at a constant 30 psi applied pressure.

Another unique feature of this flux behavior is the rather steady flux observed after 5 L/m^2 which, in the cases shown here, varied by less than 10% after the initial flux drop. This held true even for experiments with the Viresolve® Pro that went to 60 L/m^2. This flux behavior differs from what would be expected by the conventional filter fouling models, where there would be continued flux decline as a function of the volumetric throughput.

This "immediate" flux decline and the "steady" flux behavior has been highlighted recently by Bieberbach et al. who also used purified mAb therapeutics as their feed solution to study virus filtration (Bieberbach et al. 2019). Their study also contained a polyclonal IgG solution, which followed the classical filter fouling models and has a gradual and continual drop

in flux, rather than immediate drop in flux as shown by the purified mAb therapeutics. The results presented in Figure **4-1** are consistent with what has been seen for purified mAbs in their study.

The other factor when evaluating filtration performance of high value therapeutics is the transmission through the filter, or the concentration of mAb in the filtrate. Clearly, significant losses of product during filtration are undesirable. To evaluate this, the concentration of the filtrate samples collected is measured using the absorbance at 280nm.

Figure **4-2** presents the normalized mAb concentration of filtrate, the filtrate concentration divided by the feed concentration, plotted against the volumetric throughput. It is clear that all experiments performed had nearly 100% transmission, so no significant transmission issues through the virus filters.

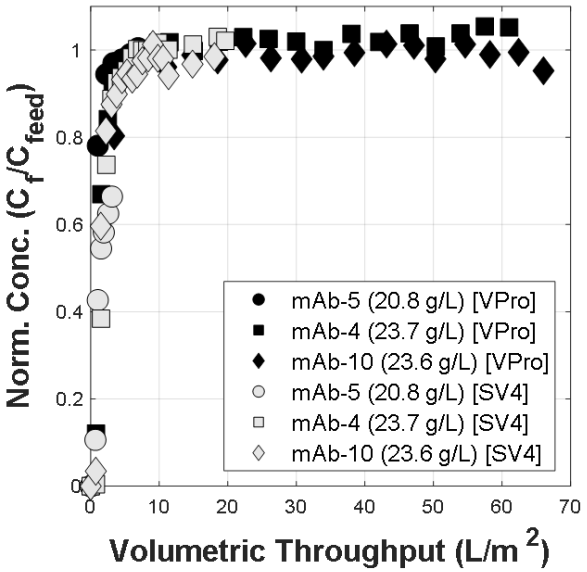

Figure **4-2**: Normalized concentration of mAb in the filtrate as a function of volumetric throughput.

The final data collected from a filtration experiment is the normalized flux through the membrane during the buffer flush immediately after the experiment. Those results give us a qualitative idea about the type of fouling present during mAb filtration. It is clear from Figure **4-**

3: that most experiments had a high recovery of flux when buffer was flushed through the filter holder. For the classical fouling mechanisms like pore blockage, cake formation, or pore constriction, a flush with the buffer in the same direction as the mAb filtration would not cause as dramatic an increase in flux as seen here. The only experiment that did not have as high a recover was mAb-5 through the Viresolve® Pro. This indicates that the mechanism of fouling for this mAb at the stock concentration of 20.8 g/L may be slightly different than the others, or more likely is that the buffer volume needed to recover the flux is higher. Although not shown here, mAb-5 at lower concentrations of 10,4,2,1 g/L all had high flux recovery, similar to the other datasets shown on Figure **4-3**.

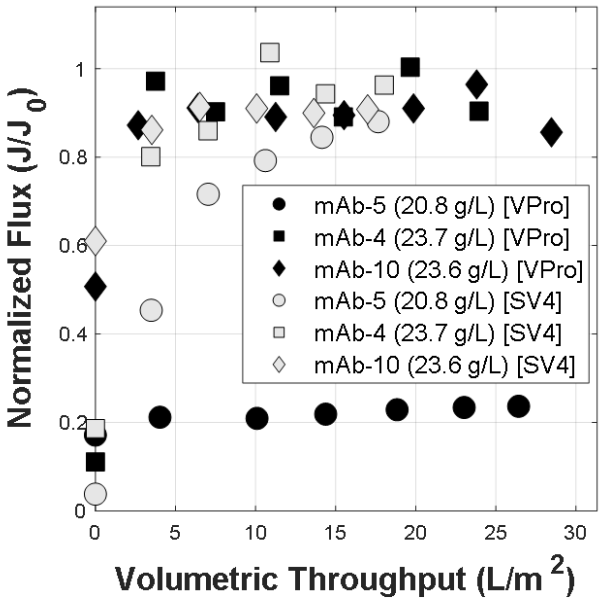

Figure **4-3**: Normalized flux of the buffer immediately after mAb filtration.

4.2 Characterization of mAbs

To better understand the mAbs in this study and their filtration behavior, the following characterization techniques were used. Previous work has shown that the presence of higher

molecular weight species (HMWS) in the feed can cause significant fouling (Bieberbach et al. 2019; Rayfield et al. 2015). The presence of HMWS caused irreversible fouling, and a gradual decline in flux. The presence and relative concentration of these HMWS can be determined using size exclusion chromatography (SEC). The results of SEC (not shown) for mAbs 4,5,and 10 did not result in the detection of any HMWS, which is consistent with the filtration behavior we have seen during mAb filtration and the following buffer flush.

Dynamic light scattering was used to measure the diffusivity and hydrodynamic size of the mAbs. The particle size distributions were all monodisperse with a polydispersity below 0.1, indicating that the cumulants analysis Z-average parameter gives a good description of the size of the particles (Malvern Instruments Ltd. 2013). Using the Stokes-Einstein relation for diffusion of a sphere in low Reynold's number fluid, shown in Equation (4-1), the average diffusivity of the particles was calculated for all three mAbs and is shown in Figure **4-4** plotted as a function of particle concentration. In Equation (4-1), D is the diffusivity, k_B is the Boltzmann constant, T is temperature, η is the viscosity of the dispersant, and r is the radius of the particle.

$$D = \frac{k_B T}{6 \pi \eta r} \qquad (4-1)$$

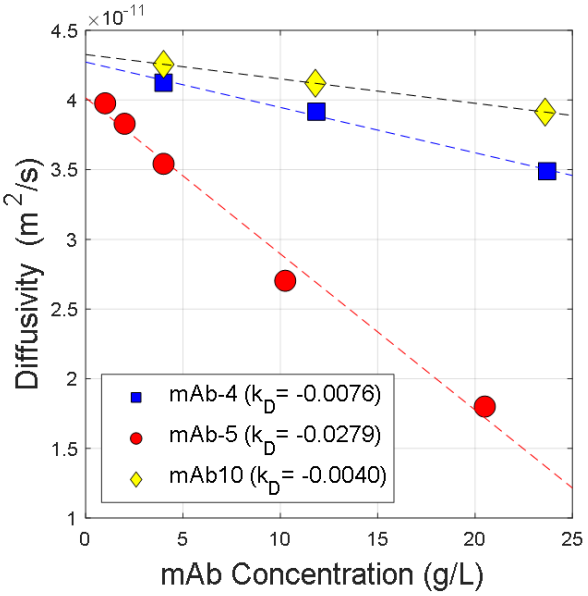

Figure **4-4**: Diffusivity of mAbs as a function of concentration. Interaction parameter k_D is specified in the legend.

The dependence of diffusivity on particle concentration can be expressed by Equation (4-2), where k_D is the interaction parameter and D_0 is the infinitely dilute case. The sign of the interaction parameter gives an indication of the intermolecular interactions affecting the mAb. All of them here are negative, meaning they have attractive interactions. The magnitude of the interaction parameter also gives an indication how strong these forces are. mAb-5 has the strongest k_D of the mAb studied, followed by mAb-4 and mAb-10 respectively.

$$D = D_0(1 + k_D C) \qquad (4-2)$$

The solution viscosity is a parameter that could impact the flux immediately, and also cause steady flux behavior during the experiment. It has been shown that attractive intermolecular interactions can cause significant increases in viscosity (Sarangapani et al. 2016; Raut and Kalonia 2016). Using capillary viscometry, the solution viscosity was estimated as shown in

Figure **4-5**. It is clear from this that the decreases in flux observed in Figure **4-1** do not match the increases in viscosity seen at the same concentrations. The viscosity measured would result in a much smaller decrease in flux. For example for mAb 5, an 80% increase in viscosity would drop the flux by 45% . We saw over 80% decline in flux, much higher than what the viscosity change would have predicted. Also, viscosity would impact the two virus filters in similar ways. So the fact that there is different behavior between the Viresolve® Pro and the Pegasus™ SV4 leads to concluding that the viscosity change is not the significant mechanism behind the flux decline.

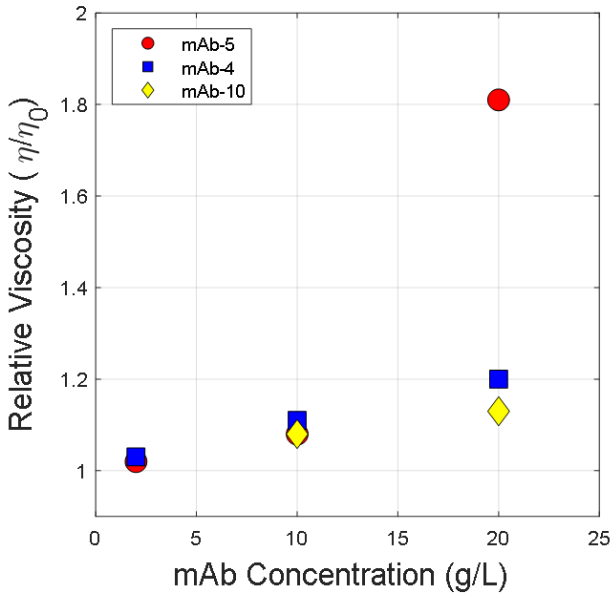

Figure **4-5**: Relative viscosity as a function of mAb concentrations.

To further investigate the cause for diffusivity increases, as well as viscosity increases, which correlate with mAb concentration, analytical hydrophobic interaction chromatography (HIC) was conducted to measure relative surface hydrophobicity of the mAbs. This technique allows for the mAb to bind to the column at high salt concentrations, then the salt concentration in the buffer is decreased over time. As the salt concentration decreases, the mAbs elute from the column. The lower the salt concentration at the time of mAb elution, the higher the surface

hydrophobicity. Since all mAbs are run with the same protocol, the longer the elution time, the higher the surface hydrophobicity. Figure **4-6** shows that mAb-5 has an elution time around 71 minutes, which is 17 minutes longer than mAb-4 and mAb-10. This indicates that mAb-5 is significantly more hydrophobic than the other mAbs in this study and may have a strong impact on the intermolecular interactions.

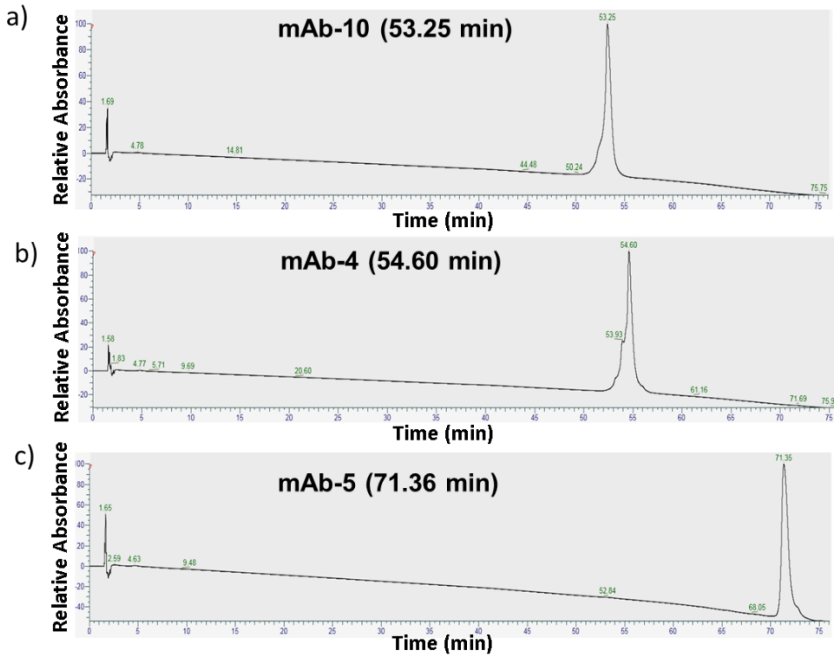

Figure **4-6**: Analytical hydrophobic interaction chromatography for a) mAb-10, b) mAb-4 and c) mAb-5.

Hydrophobic interactions qualitatively identified by HIC begin to explain the behavior seen by mAb-5. The higher magnitude negative interaction parameter of mAb-5 is consistent with a more hydrophobic mAb. Also the viscosity increases, while maybe not the major flux decline mechanism, are consistent with the more hydrophobic mAb.

4.3 Excipient effects of filtration

With a working understanding that hydrophobic interactions are contributing to the flux decline, an investigation was conducted to study known excipients that affect the hydrophobicity of mAbs. Hung et al. and Nishinami et al. identified 1.3M L-proline and 150mM hydantoin respectively as excipients which impacted the hydrophobic interactions of self-associating mAbs (Hung et al. 2018; Nishinami et al. 2019). Nishinami et al. found that hydantoin decreased viscosity of concentrated mAb solutions and that molecular dynamics simulations indicated that the hydantoin interacts with the aromatic rings of tryptophan residues.

To see this effect, the excipients weree added to mAb-5 and a virus filtration experiment was run at 30 psi. Figure **4-7** shows the effects of the addition of proline and hydantoin on mAb-5 flux through the Viresolve® Pro in panel a, and Pegasus™ SV4 in panel b. The addition of hydantoin increased initial flux through the Viresolve® Pro, which is consistent with their effects on hydrophobic interactions. The overall improvement in flux, however, for the Viresolve® Pro was small. The Pegasus™ SV4 filtration was significantly improved by the addition of hydantoin, where the flux decline was reduced from 70% to 25%. Interestingly, in both cases, the proline did not improve the flux decline at these experimental conditions.

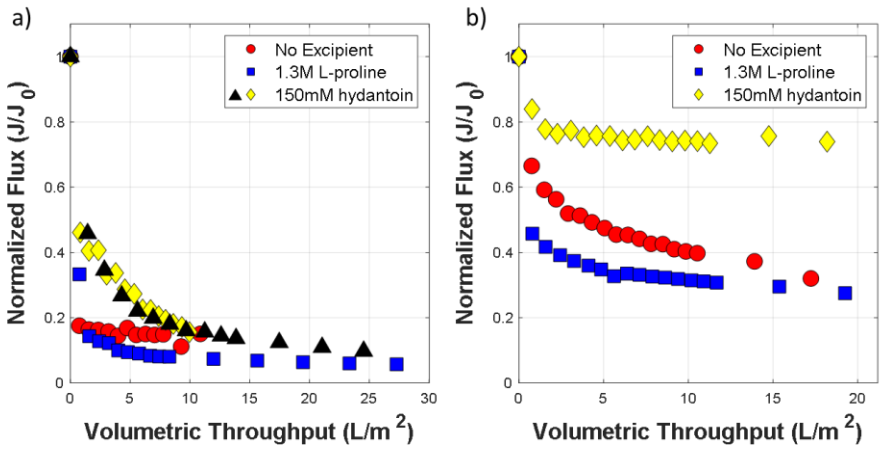

Figure **4-7**: Normalized flux plotted against volumetric throughput for filtration experiment at 30 psi. The effect of excipient additions to mAb-5 at a) 4 g/L through the Viresolve® Pro and b) 10 g/L through the Pegasus™ SV4 membrane.

4.4 Flux decline mechanism investigation

The goal of this section is to detail the investigation into the fouling mechanism for mAb-5. This mAb was used for this part due to its poor performance in filtration and to narrow the scope of work to focus on just one of the mAbs.

4.4.1 Effect of membrane orientation

Throughout this work, experiments were performed with the Viresolve pro in two different orientations, skin facing upstream in Chapter 3 to study sieving and concentration polarization effects and skin facing downstream thus far in Chapter 4 to study filtration performance in the manufacturer recommended orientation. The membrane orientation of earlier generation virus filter has been studied by Syedain et al. and changed how virus filters were designed. Early generation virus filters were actually recommended to be operated like ultrafiltration membranes with the selective skin-side facing the feed. Syedian et al. demonstrated

that the fouling mechanism of cysteinylated bovine serum albumin through a virus filter with the skin -up orientation was primarily an osmotic pressure effect while the skin-down mechanism was not driven by osmotic pressure, rather irreversible fouling within the porous structure (Syedain, Bohonak, and Zydney 2006). It is also important to note that the flux with the skin-down was significantly higher than the manufacturer recommended skin-up orientation.

While mAbs 4,5,10 used in this work do not show irreversible fouling, the differences in membrane orientation is one way of learning more about the fouling mechanisms in our system. To explore this, mAb-5 at 4 g/L feed concentration was filtered at 30 psi through the Viresolve® Pro membrane, with different orientations. The results of those experiments are shown in Figure **4-8** where a clear impact of Viresolve® Pro orientation is seen. The normal orientation not only has higher flux but also has a steady flux around 150 LMH for 20 L/m^2 of solution. The Viresolve® Pro in reverse orientation has larger initial flux decline that continues to increase during filtration. The normalized filtrate concentration of the reverse orientation does not reach the feed concentration, it approaches around 60% of the feed before beginning to level off.

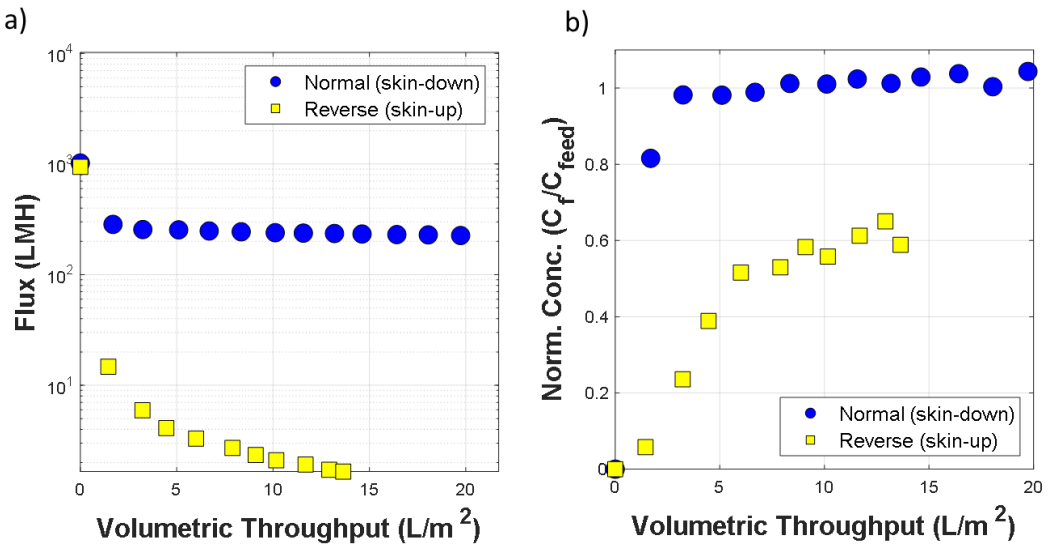

Figure **4-8**: mAb-5 at 4 g/L feed concentration filtered at 30 psi through normal (circles) and reverse (square) Viresolve® Pro. Panel a) shows the flux as a function of volumetric throughput, where the y-axis is a log-scale. Panel b) is the normalized filtrate concentration as a function of volumetric throughput.

These behaviors indicate that there is a difference in fouling mechanism when operating Viresolve® Pro in different orientations. It has been clearly demonstrated from Chapter 3 that there is significant retention of the mAb by the skin of the virus filters. It seems that the location of the concentration polarization is important and plays a role in the fouling behavior. For the normal orientation case, the concentration polarization boundary layer is within the microporous structure of the filter. For the reverse orientation case, the concentration polarization boundary layer is in the bulk solution, on top of the skin.

At this point, there are a few possibilities to describe this behavior. The support layer could be acting as a prefilter, capable of removing foulants or altering a key foulant. Another idea could be that there is some sort of mAb "gel" that forms at the skin when a high concentration is reached. This gel may be increasing the resistance to flow, and this resistance may be altered depending on where it forms, in the porous layer or in the bulk solution. Additionally, it's feasible that the gradient in pore size with Viresolve® Pro in normal orientation, as well as the porosity of the membrane decreasing rapidly when going from the porous region into the skin is increasing

the fluid velocity, and somehow altering the mAb retention. The following sections will detail some unusual filtration experiments to investigate and test these ideas. While they are not industrial solutions to reducing the flux decline, they will help identify the fouling mechanisms in these filtration systems.

4.4.2 Effect of pre-filtration on virus filter performance

To first test what is causing this flux decline, an experiment was ran where two Viresolve® Pro membranes were stacked on top of one another, separated by a 5 μm pore size nylon filter. The upstream Viresolve® Pro is oriented skin-down, while the orientation of the downstream Viresolve® Pro is either skin-down or skin-up. This nylon filter was added to act like a spacer to separate the two Viresolve® Pro skins and improve the flow through the whole system. Since the Viresolve® Pro skin has low porosity, having them right on top of each other could cause blockage of pores, the nylon prevents that from happening. The results of these experiments, shown in Figure **4-9**, indicate that the orientation of the downstream Viresolve® Pro had little effect on the normalized flux. Having a normal oriented Viresolve® Pro and the nylon spacer directly on top of the reverse Viresolve® Pro altered the fouling mechanism such that the declining flux behavior seen with reverse Viresolve® Pro is completely removed and, after the immediate drop in flux, is steady.

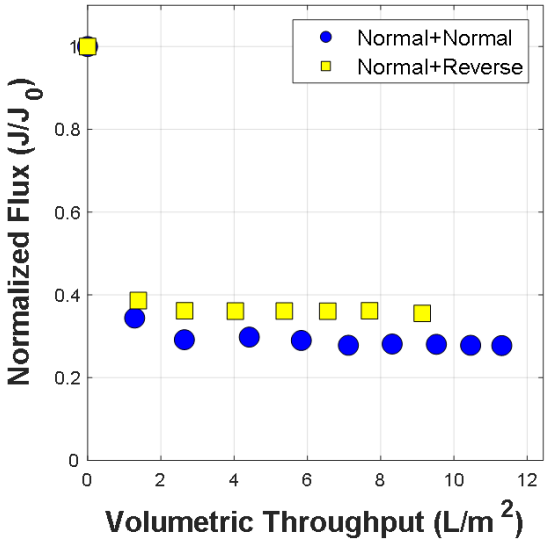

Figure **4-9**: Normalized flux plotted against volumetric throughput for double layered Viresolve® Pro, where the circle markers are the result for the filtration operated with both Viresolve® Pro in the skin-down (normal) orientation. The square markers are the result for filtration with the downstream Viresolve® Pro in the reverse orientation.

However, upon further investigating, it is not the presence of the upstream Viresolve® Pro that alters the flux behavior, the nylon filter alone is able to change the flux behavior through the reverse Viresolve® Pro from a declining flux to a steady flux. The result of this experiment is shown using upward facing triangles in Figure **4-10**. The nylon membrane did not act as a spacer, it had significant improvement in flux on it's own. In fact, the mode in which the prefiltration is operated dictates whether or not there is an improvement in flux through the reverse Viresolve® Pro. After seeing the effect of the nylon placed directly on top of the Viresolve® Pro skin (integral prefilter configuration), an experiment was conducted which consisted of pre-filtering the feed through the nylon filter, collecting the filtrate and using that as feed through a Viresolve® Pro in reverse orientation. This batch prefiltration experiment resulted in no improvement in flux through the reverse Viresolve® Pro, as seen by the down-ward facing triangles in Figure **4-10**. Another mode of pre-filtration is an in-line configuration, which entails

placing the prefilter in a separate holder, upstream of another holder with a Viresolve® Pro in reverse orientation. This configuration also failed to improve the flux, which is shown by the diamond markers in Figure **4-10**. The delayed flux decline seen for this experiment is due to the extra hold up volume between the two holders. To prevent air from passing through the filters, there is noticeable buffer hold up in the system, which delayed flux decline. However once mAb reaches the Viresolve® Pro skin, the flux declines rapidly, as if the prefilter wasn't even there.

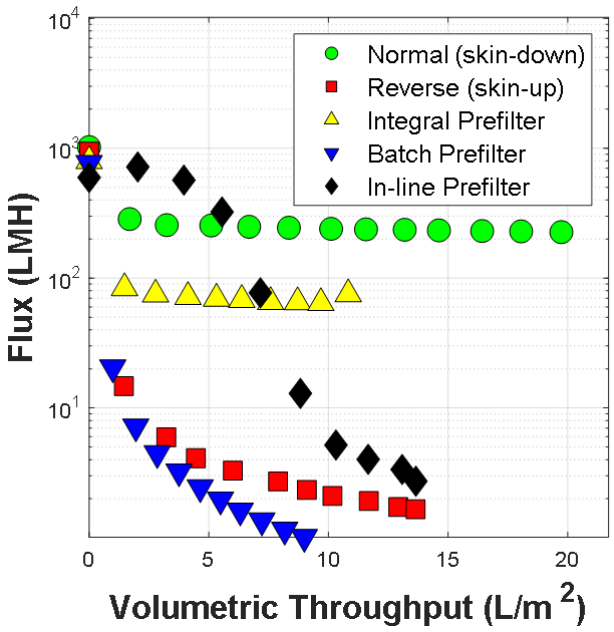

Figure **4-10**: Flux of mAb-5 at 4 g/L through reverse Viresolve® Pro with different 5 µm nylon pre-filtration configurations Batch and in-line configurations did not improve the flux like integral configuration.

It was unexpected that a large pore prefilter (250 times larger pores than the Viresolve® Pro skin), like this nylon membrane would have such a dramatic impact on flux when laid directly on top of the skin and that this affect isn't duplicated by other methods of pre-filtration. This would indicate that the prefilter is somehow altering the polarization layer or having an impact on the gel formation. This was explored further by changing the pre-filter type while maintaining the 5 µm pore size, with results shown in Figure **4-10**. The Isopore membrane which

is a track-etched polycarbonate membrane (downward facing triangles) had little impact on the flux. This is compared to the Durapore membrane which is a polyvinylidene fluoride (PVDF) membrane that (diamond markers) improved flux more than the nylon by a factor of four. The Durapore at this pore size actually performed better than the Viresolve® Pro operated in it's normal orientation (skin-side down). This suggests that the prefilter chemistry or morphology is at least as important as the pore size.

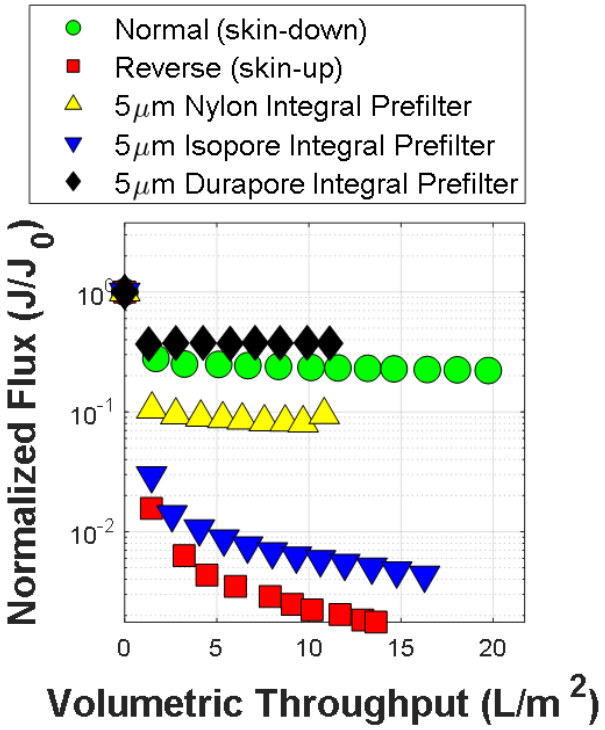

Figure **4-11**: Normalized flux plotted against the volumetric throughput for different pre-filters used in the integral configuration.

The Durapore prefilter is available in a variety of pore sizes. Figure **4-12** shows the normalized flux when varying the pore size from 0.1 to 5 μm. All of the Durapore prefilters when used as integral prefilters were capable of creating steady flux behavior, however the flux decline was affected. Interestingly, the flux is higher with increasing pore size. The 0.1 μm pore size Durapore had normalized flux of 0.02, whereas the 5 μm Durapore had normalized flux of 0.3,

which was over a factor of 10 higher. The white circle markers have the prefilter integral to normal oriented Viresolve® Pro, as a check to show that the prefilter does not impact the flux through this filter, and interestingly does increase the normalized flux slightly. Indicating that the affect of the prefilter was seen even when placed on top of the porous microstructure of the Viresolve® Pro.

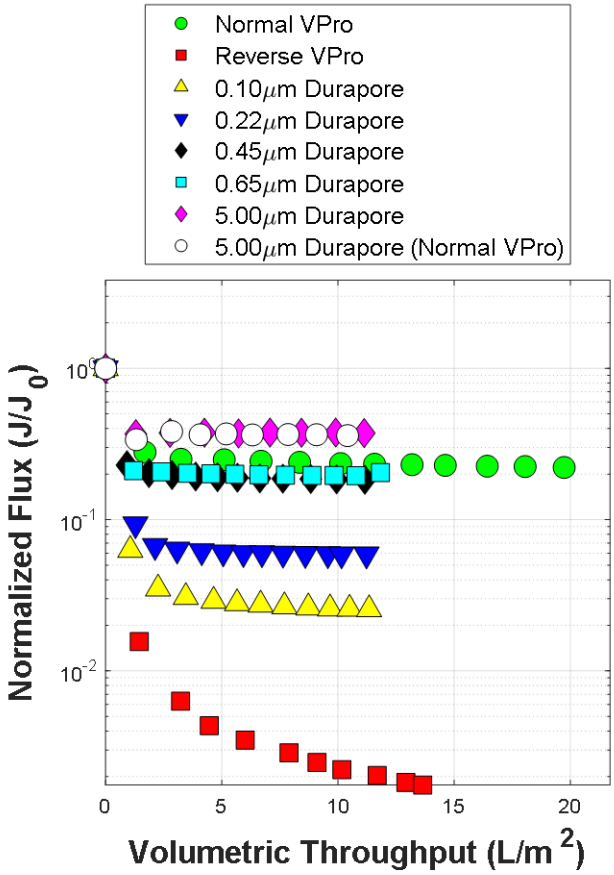

Figure **4-12**: Effect of integral prefilter pore size shown as normalized flux plotted against the volumetric throughput.

To develop a better understanding of the fouling mechanism, specifically what is contributing to the degree of flux decline, a series of experiments were done which involve layering the 5 μm and 0.1 μm Durapore prefilters upstream of the reverse Viresolve® Pro. The order of the pre-filter layers, whether the feed passes through the 5 or 0.1 μm prefilter first or

second has no impact on the flux decline. This result is demonstrated in Figure **4-13**Figure **4-12** and indicates that the pore size of the prefilter where the concentration polarization occurs does not control the flux decline. As long as the 5 µm Durapore is a layer in the multi-layer system, the flux decline will match the flux decline of the 5 µm Durapore alone. This is consistent with the results from Figure **4-12** showing performance of the 5 µm Durapore prefilter enhancing the flux regardless of Viresolve® Pro orientation.

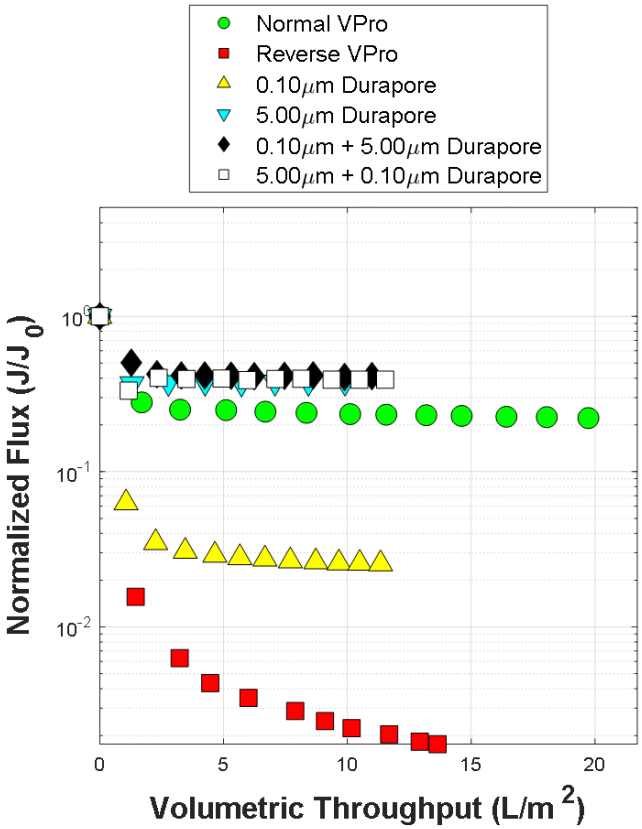

Figure **4-13**: Normalized flux plotted against the volumetric throughput for layering 5 and 0.1 µm Durapore integral pre-filter experiments.

The multi-layer stack shown previously contains layers that, each layer alone, would change the flux behavior of the reverse Viresolve® Pro from declining to steady. To find a true spacer to separate the pre-filter and the Viresolve® Pro skin, a 180 µm nylon net was used. This filter alone did not improve the flux behavior at all from the reverse Viresolve® Pro case without

any filter upstream, as shown by the downward facing triangles in Figure **4-14**. The addition of this spacer between the 5 µm Durapore and the Viresolve® Pro skin resulted in the same flux decline as if the spacer was not there.

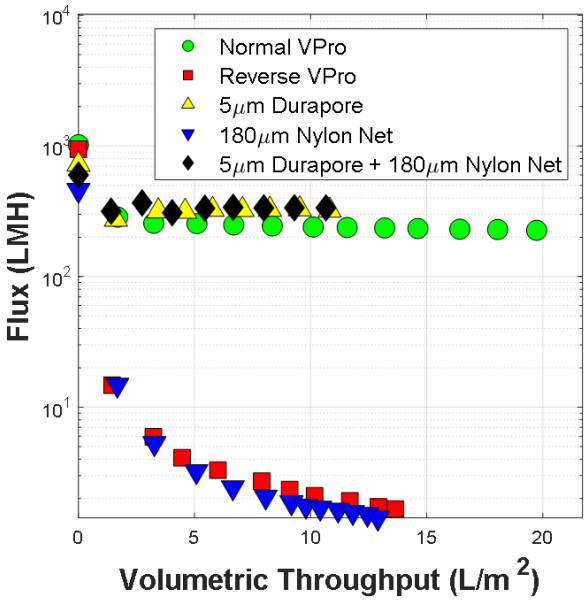

Figure **4-14**: Flux plotted against volumetric throughput for a series of experiments studying the effects of adding a 180 µm nylon net between the 5 µm Durapore prefilter and reverse oriented Viresolve® Pro.

Based on this series of prefiltration experiments, the possible flux mechanism can be narrowed down, but not entirely confirmed. It can be said with certainty that polarization within the prefilter is not significant. It is clear that polarizations occurs in different microporous environments, but the environment in which a possible "gel" is forming does not impact the flux decline mechanism. With the evidence from the nylon net spacer experiments, it's unlikely that there is some sort of unique flow pattern and increase in velocity that is decreasing mAb retention and increasing flux. This leaves some type of foulant removal or modification by the prefilter that is impacting the flux behavior. This effect must be somehow reversible, because previous in-line

prefiltration results showed no improvement. The nylon net spacer has very short time between prefilter and Viresolve® Pro skin.

4.4.3 Residence time between prefilter and Viresolve® Pro skin

To see if there is some sort of reversible foulant formation, the goal is to vary the residence time of the integral and inline prefiltration experiments. To alter the residence time between prefilter and skin, the pressure applied to the system can be modified as well as the hold-up volume between prefilter exit and Viresolve® Pro skin. To calculate the hold up volumes for the integral prefiltration systems, the void volume of the nylon net spacer is determined. Given the properties of the nylon net, namely the diameter of 25 mm, depth of 0.12 mm and a porosity of 0.47, the void volume was estimated to be 0.028 mL. Therefore, the residence time can be calculated by dividing the hold-up volume by the volumetric flow rate at 10 $\mathrm{L/m^2}$ to estimate the residence time. We can alter the hold up volume in this setup by adding nylon net spacers between the prefilter and reverse Viresolve® Pro within the same membrane holder. The results of these experiments are shown in Figure **4-15**, where the number of nylon net spacers varied from 1 to 4 and the applied pressure varied from 30 psi to 1.46 psi. The residence time (RT) in seconds for each experiment is also listed in the legend.

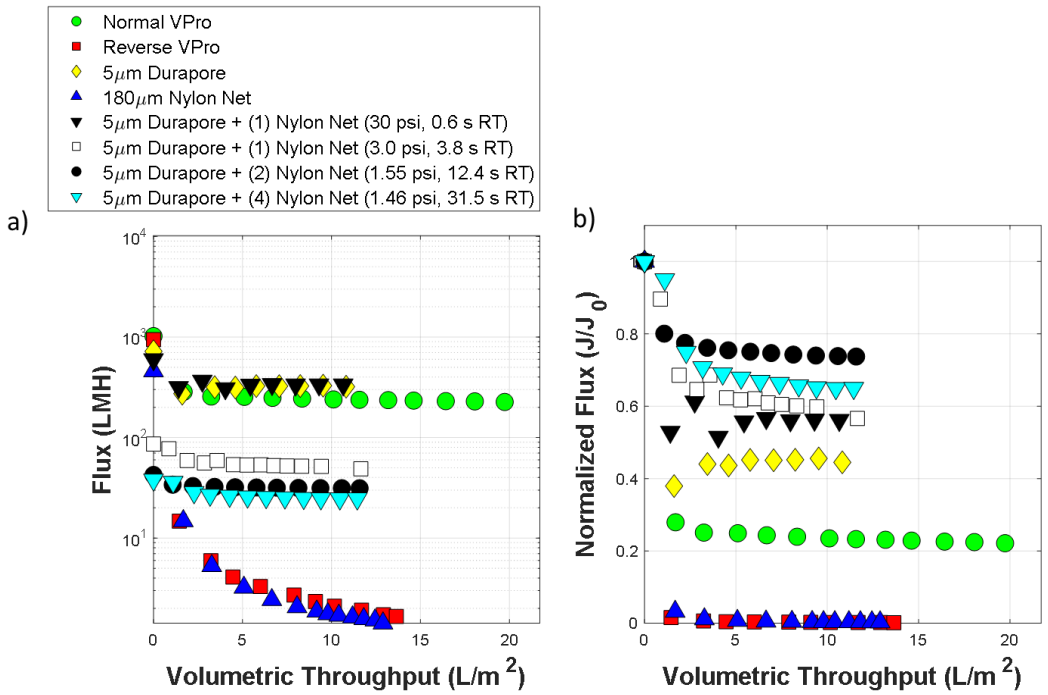

Figure **4-15**: a) Flux and b) normalized flux plotted against volumetric throughput for experiments which varied the number of nylon net spacers and decreased the applied pressure to increase residence time.

The black downward facing triangles are with one nylon net and 30 psi applied pressure. With these conditions, the residence time was 0.6 seconds. By increasing the number of nylon nets to 4 and decreasing the pressure to 1.46 psi, the residence time was decreased to 31.5 seconds, shown with light blue downward facing triangles. We can see that this experiment had steady flux behavior while being significantly lower due to the decreased applied pressure. Interestingly the normalized flux shown in panel b) is higher for the lower pressure experiments.

To add, in-line prefiltration experiments were conducted with a hold up volume of 1.4 mL, which was achieved by connecting a small plastic holder directly to the outlet of the stainless-steel holder. This allowed the membranes to be in separate holders but the hold-up volume to be minimized. The residence time for these experiments, many of which resulted in

declining flux behavior as seen in Figure **4-16**, had very high values because of the extremely low flux at 10 $\mathrm{L/m^2}$ where the residence time estimation is calculated.

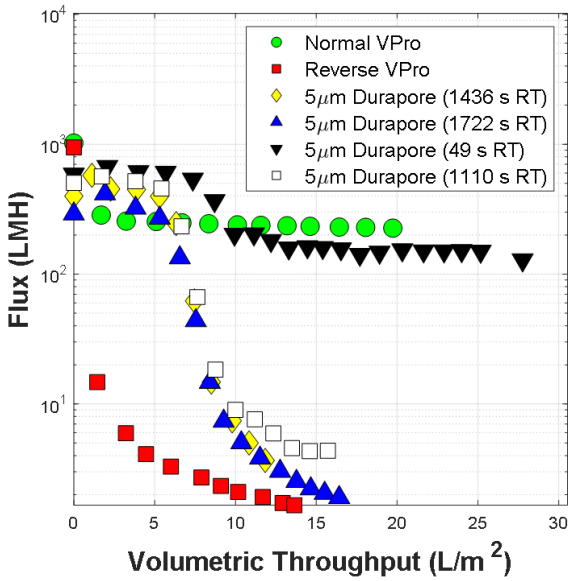

Figure **4-16**: Flux plotted against volumetric throughput for in-line prefiltration experiments.

For the in-line prefiltration experiment that did not have declining flux (downward facing black triangles), the residence time at 10 $\mathrm{L/m^2}$ is listed in the legend as 49 seconds. Due to the delay in flux decline due to buffer hold up dilutions, a better estimation would be at 15 $\mathrm{L/m^2}$, which results in a 62 second residence time. This experiment showed that an in-line set up, with adequate flux and minimized hold-up can achieve a steady flux behavior. To summarize the prefiltration experiments, both integral and in-line setups, the normalized flux at 10 $\mathrm{L/m^2}$ was plotted against the residence time determined at this flux at this volume throughput. Figure **4-17** shows this data, where the square markers are the integral experiments and the circle markers are in-line experiments.

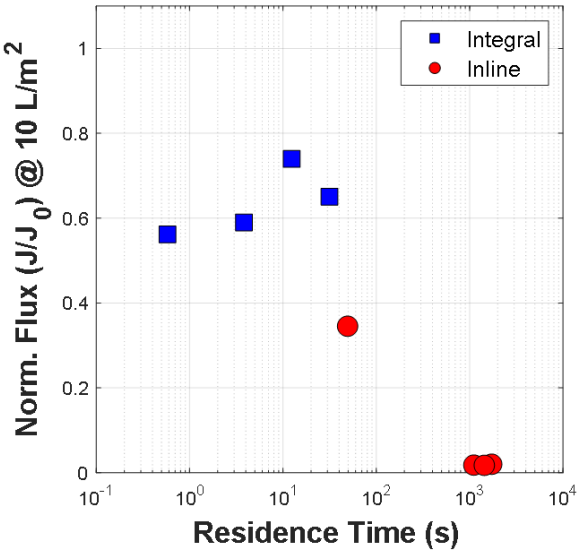

Figure **4-17**: Normalized flux at 10 L/m^2 plotted against the residence time calculated using the flux at 10 L/m^2.

After investigating the effects of residence time on filtration behavior, it seems clear that if the residence time during mAb filtration can be reduced to less than a minute, the flux behavior through the Viresolve® Pro will be steady. Based on these results, there is evidence to support the theory that the prefilter or porous microstructure of normal oriented Viresolve® Pro can affect a major foulant. Reversible self-association, something that occurs in mAbs with attractive forces, may be responsible for this behavior. When the feed passes through the prefilter or microporous support of Viresolve® Pro in normal orientation, the self-association is disrupted. If the mAb reassociates before going through the Viresolve® Pro skin, it will cause declining flux and dramatic decrease in performance. If, however, the residence time is small enough between pre-filter and Viresolve® Pro skin, the mAbs can pass through before re-clustering.

To see the generalizability of this theory, the 5 μm Durapore was used as an integral prefilter on a normal oriented Pegasus™ SV4 membrane, which is thought to have a more homogenous pore size through the depth of the filter. mAb-5 at 20.5 g/L was filtered through

Pegasus™ SV4 in the normal orientation with the skin-side down at 30psi. Figure **4-18** shows an experiment with no excipient or prefilter (triangles) showing declining flux behavior.

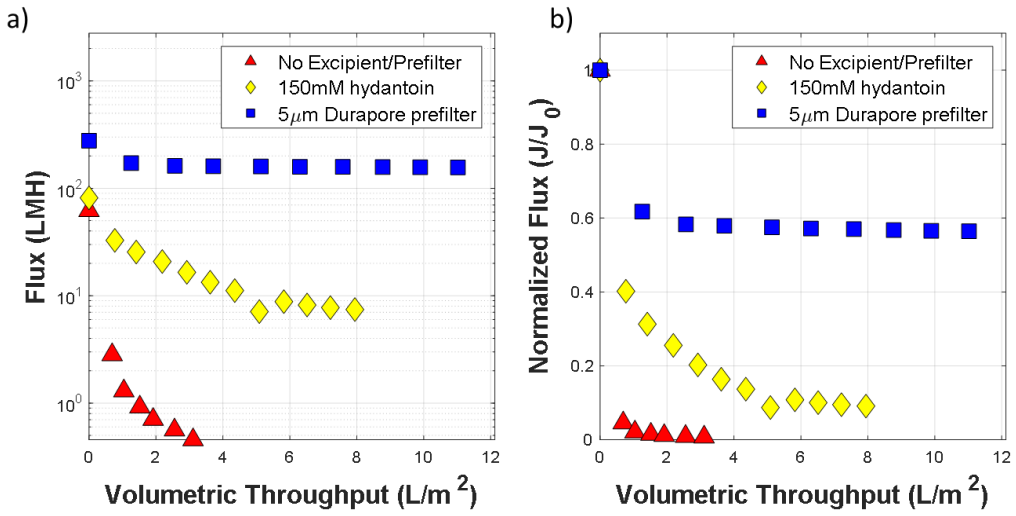

Figure **4-18**: a) Flux and b) normalized flux plotted against volumetric throughput for mAb-5 at 20.5 g/L at 30 psi through the Pegasus™ SV4 oriented with the skin-down.

The addition of 150 mM hydantoin improved the flux behavior to a steady behavior (diamonds), but still had very low flux, around 8 LMH. The addition of integral prefilter improved the flux to 160 LMH and normalized flux to 0.6 (squares). It's important to note that the prefilter had this dramatic impact on the flux behavior for the Pegasus™ SV4 in the normal orientation. The normal orientation Pegasus™ SV4, without any prefilter, had declining flux which is similar to the reverse Viresolve® Pro. The influence of the prefilter here is consistent with the proposed mechanism describing the behavior through the Viresolve® Pro. The prefilter disrupts the self-association of mAbs which would cause severe fouling if not altered.

The evidence for this fouling mechanism has never been published and the thorough investigations here disprove many of the other possible fouling mechanisms for virus filtration of mAbs. It would be overreaching to state that this mechanism is the primary fouling mechanism for all virus filtration experiments. The presence of HMWS undoubtedly has a profound impact

on flux decline, and concentration polarization occurs at the skin. However in this work, those were not the driving forces. Other previous work did have those mechanisms at play, which did not allow for investigation into the fouling mechanism that is driving this flux decline.

The role of the porous microstructure found in asymmetric virus filters has long been understood to filter out any large undissolved aggregates, and keep them from plugging the skin of the virus filter. This is certainly possible, but the microstructure also has an incredibly important function of disrupting clustering of self-associating mAbs. If this function is not achieved, as seen by a more symmetric virus filters without this porous layer, the flux crashes and the filter is not a viable solution for self-associating mAbs.

Chapter 5

Conclusions

5.1 Antibody retention by virus filtration membranes

This study presents some of the first quantitative data for the actual sieving coefficient of a monoclonal antibody through two commercial virus filtration membranes: the highly asymmetric Viresolve® Pro and the relatively homogeneous Pegasus™ SV4. Experiments were performed in a stirred ultrafiltration device to control the extent of concentration polarization, with the wall concentration evaluated based on the filtrate flux using a correlation for the osmotic pressure of the antibody solution as a function of the antibody concentration. This allowed us to directly evaluate the actual sieving coefficient for the skin layer of the Viresolve® Pro and Pegasus™ SV4 without having to use any assumed correlations for the mass transfer coefficient in the stirred cell. In addition, data obtained with the SV4 oriented with the shiny-side down demonstrated that this membrane is somewhat asymmetric, with the actual sieving coefficient of the shiny-side being around a factor of 2-4 less than that for the more open side.

Both the Viresolve® Pro and Pegasus™ SV4 virus filters show very high retention of the antibody, with actual sieving coefficients around $S_a = 0.01$ at an antibody concentration of 150 g/L. The actual sieving coefficient decreases with increasing antibody concentration going from around 0.05 at a wall concentration of 20 g/L to only $S_a = 0.005$ at $C_{wall} \approx 250$ g/L (for the Viresolve® Pro), consistent with the presence of strong intermolecular attractive interactions as described by the large negative value of k_D determined from dynamic light scattering data.

Previous studies have shown that the selectivity of the two-layer commercial Viresolve® Pro filter is close to 10^6, with nearly 100% recovery of an antibody product with a virus transmission on the order of 10^{-6} (corresponding to an LRV = $-\log_{10}S_{virus}$ = 6). However, this is only an observed selectivity. The high antibody recovery is a direct result of the high degree of antibody concentration polarization (which occurs inside the support structure of the asymmetric membrane when used with the skin-side away from the feed) at the high filtrate flux used with the Viresolve® Pro (typically on the order of 500 LMH). The actual selectivity of a single-layer of the Viresolve® Pro is only about 10-fold ($S_{mAb} \approx 0.01$ with $S_{virus} \approx 0.001$). This is consistent with predictions of available hydrodynamic models assuming a log-normal pore size distribution with coefficient of variation ($\sigma_{\ln \bar{r}}$) equal to 0.2 based on the two-fold difference in size between the antibody and virus and the reduction in S_a with increasing antibody concentration. The actual sieving coefficient of the two-layer composite Viresolve® Pro should be very similar to that for a single layer membrane as described by Boyd and Zydney (1997). In contrast, virus retention by the two-layer Viresolve® Pro will be approximately equal to the sum of the LRV for the two layers since the viruses are physically captured within the pore structure of each layer of the filter. These results provide important insights into the transport properties of virus filtration membranes used in bioprocessing.

5.2 Flux decline mechanism investigations

Filtration experiments using two different virus filters and 3 different mAbs demonstrated the importance of both the properties of the filter and the antibody solution on the filtrate flux during antibody filtration through these virus retentive membrane. In most cases, there is an immediate flux decline, followed by a steady flux during the rest of the filtration, which is in

sharp contrast to the continued flux decline observed during most filtration processes (and described by all of the classical fouling models). The observed flux decline with the antibody solutions was almost completely reversible, with the flux recovering to around 90% or greater of the initial buffer flux simply after flushing the membrane with buffer. The mAb with the lowest flux had the largest effective size (as determined by dynamic light scattering) and the strongest attractive interaction parameter (determined from the dependence of D_{eff} on the antibody concentration). This behavior was consistent with the greater surface hydrophobicity of this mAb as determined by analytical hydrophobic interaction chromatography.

The underlying pore morphology of the virus filter is also critical to mAb filtration performance. This was highlighted by examining the filtrate flux with different orientations of the asymmetric Viresolve® Pro membrane, with the flux in the skin-up orientation being 100-fold larger than that in the normal skin-down orientation . The addition of a prefilter on top of the Viresolve® Pro (with skin side up) significantly increased the filtrate flux, but only when the prefilter was almost directly on top of the virus filter. Prefiltration of the antibody solution in a batch mode provided no measurable improvement in the flux, nor did the use of an in-line prefiltration using both filter in separate holders.

Our hypothesis was that prefiltration was disrupting some foulant species present in the feed, most likely weakly associated aggregates of the monoclonal antibody. This behavior was confirmed by performing experiments in which the hold-up volume (or residence time) between the pre-filter and the virus filter was reduced to at or below one minute, with the filtrate flux under these conditions approaching that of the normal Viresolve® Pro membrane. This work provides the first demonstration that there is a critical residence time for antibody re-association and that this plays a dramatic role in determining the filtrate flux during filtration of the antibody solution through virus retentive membranes.

5.3 Recommendations

Although the data obtained in this thesis provide important insights into the reversible fouling mechanism, a more complete validation of the underlying hypothesis would require direct measurements of the break-up and re-association of the antibody clusters that are thought to control the filtrate flux behavior. One potential option would be to use an inline multi-angle light scattering (MALS) detector, similar to those employed in SEC-MALS systems (size exclusion chromatography coupled to MALS) (Patapoff, Mrsny, and Lee 1993). In this case, the antibody solution would be passed through a prefilter that has been shown to protect the virus filter from fouling, e.g., the 5 μm pore size Durapore membrane, with the permeate taken directly to the MALS detector. By varying the length of tubing between the prefilter and the MALS, one should be able to measure the effective size of the antibody solution (a measure of the degree of self-association) as a function of the residence time between the prefilter and the detector, allowing us to directly observe the re-association of the antibodies. These experiments could be performed in the presence of different buffers / excipients that are known to affect the strength of the intermolecular attractive interactions to provide additional molecular insights into the self-association behavior.

Alternatively, it might be possible to study antibody association using fluorescence resonance energy transfer (FRET), similar to the approach used by Levi and Gonzalez Flecha to study the reversible dimerization of bovine serum albumin (Levi and Gonzalez Flecha 2002). In this case, a mixture of antibodies labeled with two different fluorescent dyes would be passed through the prefilter, with the fluorescence evaluated for permeate samples as a function of time. The change in the FRET signal should be directly related to the re-association of the antibodies in solution.

It is also important to extend our work on the prefiltration / antibody self-association to other monoclonal antibodies to obtain additional insights into the factors controlling the initial fouling. This would include further investigations into the hydrophobicity and extent of self-association of the antibodies and the correlation of these parameters with the flux behavior. This could potentially lead to the development of appropriate models that could be used to predict the flux decline through different virus filters as a function of the antibody properties. This would be an extremely powerful tool that would change the process development strategy used for virus filtration steps and could lead to significant improvements in both virus filtration membranes and operating principles for more effective downstream processing of these critically important biologics.

References

Adamski, R. P., and J. L. Anderson. 1983. “Solute Concentration Effect on Osmotic Reflection Coefficient.” *Biophysical Journal* 44 (1): 79–90. https://doi.org/10.1016/S0006-3495(83)84279-9.

Baek, Youngbin, Nripen Singh, Abhiram Arunkumar, Michael Borys, Zheng J. Li, and Andrew L. Zydney. 2017. “Ultrafiltration Behavior of Monoclonal Antibodies and Fc-Fusion Proteins: Effects of Physical Properties.” *Biotechnology and Bioengineering* 114 (9): 2057–65. https://doi.org/10.1002/bit.26326.

Baek, Youngbin, Nripen Singh, Abhiram Arunkumar, and Andrew L. Zydney. 2017. “Effects of Histidine and Sucrose on the Biophysical Properties of a Monoclonal Antibody.” *Pharmaceutical Research* 34 (3): 629–39. https://doi.org/10.1007/s11095-016-2092-0.

Bakhshayeshi, Meisam, Dharmesh M Kanani, Amit Mehta, Robert Van Reis, Ralf Kuriyel, Nigel Jackson, and Andrew L Zydney. 2011. “Dextran Sieving Test for Characterization of Virus Filtration Membranes.” *Journal of Membrane Science* 379 (1–2): 239–48. https://doi.org/10.1016/j.memsci.2011.05.067.

Bakhshayeshi, Meisam, and Andrew L. Zydney. 2008. “Effect of Solution PH on Protein Transmission and Membrane Capacity during Virus Filtration.” *Biotechnology and Bioengineering* 100 (1): 108–17. https://doi.org/10.1002/bit.21735.

Bieberbach, Marc, Peter Kosiol, Alexander Seay, Moritz Bennecke, Björn Hansmann, Stefan Hepbildikler, and Volkmar Thom. 2019. “Investigation of Fouling Mechanisms of Virus Filters during the Filtration of Protein Solutions Using a High Throughput Filtration Screening Device.” *Biotechnology Progress*, 1–10. https://doi.org/10.1002/btpr.2776.

Binabaji, Elaheh, Suma Rao, and Andrew L. Zydney. 2014. “The Osmotic Pressure of Highly Concentrated Monoclonal Antibody Solutions: Effect of Solution Conditions.” *Biotechnology and Bioengineering* 111 (3): 529–36. https://doi.org/10.1002/bit.25104.

Blatt, William F, Arun Dravid, Alan S Michaels, and Lita Nelsen. 1970. “Solute Polarization and Cake Formation in Membrane Ultrafiltration: Causes, Consequences, and Control Techniques.” In *Membrane Science and Technology: Industrial, Biological, and Waste Treatment Processes*, edited by James E Flinn, 47–97. Boston, MA: Springer US. https://doi.org/10.1007/978-1-4684-1851-4_4.

Bolton, Glen, Mark Cabatingan, Mike Rubino, Scott Lute, Kurt Brorson, and Mark Bailey. 2005. “Normal-Flow Virus Filtration: Detection and Assessment of the Endpoint in Bioprocessing.” *Biotechnology and Applied Biochemistry* 42 (2): 133. https://doi.org/10.1042/BA20050056.

Burnouf, Thierry, and M. Radosevich. 2003. “Nanofiltration of Plasma-Derived Biopharmaceutical Products.” *Haemophilia* 9 (1): 24–37. https://doi.org/10.1046/j.1365-2516.2003.00701.x.

David, Laura, Jens Niklas, Bastian Budde, Martin Lobedann, and Gerhard Schembecker. 2019. “Continuous Viral Filtration for the Production of Monoclonal Antibodies.” *Chemical Engineering Research and Design* 152: 336–47. https://doi.org/10.1016/j.cherd.2019.09.040.

Deen, W. M. 1987. “Hindered Transport of Large Molecules in Liquid-filled Pores.” *AIChE Journal* 33 (9): 1409–25. https://doi.org/10.1002/aic.690330902.

Fallahianbijan, Fatemeh, Sal Giglia, Christina Carbrello, and Andrew L. Zydney. 2017. “Use of Fluorescently-Labeled Nanoparticles to Study Pore Morphology and Virus Capture in Virus Filtration Membranes.” *Journal of Membrane Science* 536 (April): 52–58. https://doi.org/10.1016/j.memsci.2017.04.066.

FDA. 1998. “Guidance for Industry Q5A Viral Safety Evaluation of Biotechnology Products Derived From Cell Lines of Human or Animal Origin.” *International Conference of Harmonization* 20857 (September): 301–827. http://www.fda.gov/cder/guidance/index.htm%0Ahttp://www.fda.gov/cder/guidance/index.htm.

Hadidi, Mahsa, John J. Buckley, and Andrew L. Zydney. 2015. “Ultrafiltration Behavior of Bacterial Polysaccharides Used in Vaccines.” *Journal of Membrane Science* 490: 294–300.

https://doi.org/10.1016/j.memsci.2015.04.047.

Hongo-Hirasaki, Tomoko, Masayasu Komuro, and Shoichi Ide. 2010. “Effect of Antibody Solution Conditions on Filter Performance for Virus Removal Filter PlanovaTM 20N.” *Biotechnology Progress* 26 (4): 1080–87. https://doi.org/10.1002/btpr.415.

Hung, Jessica J., Barton J. Dear, Aileen K. Dinin, Ameya U. Borwankar, Sumarth K. Mehta, Thomas T. Truskett, and Keith P. Johnston. 2018. “Improving Viscosity and Stability of a Highly Concentrated Monoclonal Antibody Solution with Concentrated Proline.” *Pharmaceutical Research* 35 (7): 133. https://doi.org/10.1007/s11095-018-2398-1.

Kedem, O., and A. Katchalsky. 1958. “Thermodynamic Analysis of the Permeability of Biological Membranes to Non-Electrolytes.” *BBA - Biochimica et Biophysica Acta* 27 (C): 229–46. https://doi.org/10.1016/0006-3002(58)90330-5.

Kosiol, Peter, Marie Theres Müller, Benjamin Schneider, Björn Hansmann, Volkmar Thom, and Mathias Ulbricht. 2018. “Determination of Pore Size Gradients of Virus Filtration Membranes Using Gold Nanoparticles and Their Relation to Fouling with Protein Containing Feed Streams.” *Journal of Membrane Science* 548 (May 2017): 598–608. https://doi.org/10.1016/j.memsci.2017.11.048.

Leisi, Remo, Jan Bieri, Nathan J. Roth, and Carlos Ros. 2020. “Determination of Parvovirus Retention Profiles in Virus Filter Membranes Using Laser Scanning Microscopy.” *Journal of Membrane Science* 603: 118012. https://doi.org/10.1016/j.memsci.2020.118012.

Levi, Valeria, and F. Luis Gonzalez Flecha. 2002. “Reversible Fast-Dimerization of Bovine Serum Albumin Detected by Fluorescence Resonance Energy Transfer.” *Biochemica et Biophysica Acta*, no. 1599: 141–48.

Lute, Scott, Mark Bailey, Jessica Combs, Muppalla Sukumar, and Kurt Brorson. 2007. “Phage Passage after Extended Processing in Small-Virus-Retentive Filters.” *Biotechnology and Applied Biochemistry* 47 (3): 141. https://doi.org/10.1042/ba20060254.

Malvern Instruments Ltd. 2013. “Zetasizer Nano User Manual MAN0485,” no. 1.1 (May).

Marques, Bruno F., David J. Roush, and Kent E. Göklen. 2009. “Virus Filtration of High-Concentration Monoclonal Antibody Solutions.” *Biotechnology Progress* 25 (2): 483–91. https://doi.org/10.1002/btpr.177.

Mitchell, Brent D., and William M. Deen. 1986. “Effect of Concentration on the Rejection Coefficients of Rigid Macromolecules in Track-Etch Membranes.” *Journal of Colloid And Interface Science* 113 (1): 132–42. https://doi.org/10.1016/0021-9797(86)90213-4.

Mochizuki, Seiichi, and Andrew L. Zydney. 1993. “Theoretical Analysis of Pore Size Distribution Effects on Membrane Transport.” *Journal of Membrane Science* 82 (3): 211–27. https://doi.org/10.1016/0376-7388(93)85186-Z.

Nazem-Bokaee, Hadi, Fatemeh Fallahianbijan, Dayue Chen, Sean Michael O’Donnell, Christina Carbrello, Sal Giglia, David Bell, and Andrew L. Zydney. 2018. “Probing Pore Structure of Virus Filters Using Scanning Electron Microscopy with Gold Nanoparticles.” *Journal of Membrane Science* 552 (February): 144–52. https://doi.org/10.1016/j.memsci.2018.01.069.

Nishinami, Suguru, Tomoshi Kameda, Tsutomu Arakawa, and Kentaro Shiraki. 2019. “Hydantoin and Its Derivatives Reduce the Viscosity of Concentrated Antibody Formulations by Inhibiting Associations via Hydrophobic Amino Acid Residues.” *Industrial and Engineering Chemistry Research* 58 (36): 16296–306. https://doi.org/10.1021/acs.iecr.9b01739.

Opong, W. Senyo, and Andrew L. Zydney. 1991. “Diffusive and Convective Protein Transport through Asymmetric Membranes.” *AIChE Journal* 37 (10): 1497–1510. https://doi.org/10.1002/aic.690371007.

Patapoff, T.W., R.J. Mrsny, and W.A. Lee. 1993. “The Application of Size Exclusion Chromatography and Computer Simulation to Study the Thermodynamic and Kinetic Parameters for Short-Lived Dissociable Protein Aggregates.” *Analytical Biochemistry* 212 (1): 71–78. https://doi.org/10.1006/abio.1993.1293.

Raut, Ashlesha S., and Devendra S. Kalonia. 2016. “Viscosity Analysis of Dual Variable Domain Immunoglobulin Protein Solutions: Role of Size, Electroviscous Effect and Protein-Protein Interactions.” *Pharmaceutical Research* 33 (1): 155–66. https://doi.org/10.1007/s11095-015-1772-5.

Rayfield, William J., David J. Roush, Rebecca A. Chmielowski, Nihal Tugcu, Shehab Barakat, and Jason K. Cheung. 2015. "Prediction of Viral Filtration Performance of Monoclonal Antibodies Based on Biophysical Properties of Feed." *Biotechnology Progress* 31 (3): 765–74. https://doi.org/10.1002/btpr.2094.

Ruanjaikaen, Krisada, and Andrew L. Zydney. 2013. "Intermolecular Interactions during Ultrafiltration of Pegylated Proteins." *Biotechnology Progress* 29 (3): 655–63. https://doi.org/10.1002/btpr.1709.

Sarangapani, Prasad S., Justin Weaver, Arun Parupudi, Tabot M.D. Besong, Gary G. Adams, Stephen E. Harding, Prakash Manikwar, Maria M. Castellanos, Steven M. Bishop, and Jai A. Pathak. 2016. "Both Reversible Self-Association and Structural Changes Underpin Molecular Viscoelasticity of MAb Solutions." *Journal of Pharmaceutical Sciences* 105 (12): 3496–3506. https://doi.org/10.1016/j.xphs.2016.08.020.

Sommerfeld, Sven, and Jochen Strube. 2005. "Challenges in Biotechnology Production - Generic Processes and Process Optimization for Monoclonal Antibodies." *Chemical Engineering and Processing: Process Intensification* 44 (10): 1123–37. https://doi.org/10.1016/j.cep.2005.03.006.

Suzuki, Masami, Chie Kato, and Atsuhiko Kato. 2015. "Therapeutic Antibodies: Their Mechanisms of Action and the Pathological Findings They Induce in Toxicity Studies." *Journal of Toxicologic Pathology* 28 (3): 133–39. https://doi.org/10.1293/tox.2015-0031.

Syedain, Zeeshan H., David M. Bohonak, and Andrew L. Zydney. 2006. "Protein Fouling of Virus Filtration Membranes: Effects of Membrane Orientation and Operating Conditions." *Biotechnology Progress* 22 (4): 1163–69. https://doi.org/10.1021/bp050350v.

Vilker, Vincent L., Clark K. Colton, and Kenneth A. Smith. 1981. "The Osmotic Pressure of Concentrated Protein Solutions: Effect of Concentration and Ph in Saline Solutions of Bovine Serum Albumin." *Journal of Colloid And Interface Science* 79 (2): 548–66. https://doi.org/10.1016/0021-9797(81)90106-5.

Wickramasinghe, S. R., Emily D. Stump, David L. Grzenia, Scott M. Husson, and John Pellegrino. 2010. "Understanding Virus Filtration Membrane Performance." *Journal of Membrane Science* 365 (1–2): 160–69. https://doi.org/10.1016/j.memsci.2010.09.002.

Zeman, Leos J., and Andrew L. Zydney. 1996. *Microfiltration and Ultrafiltration*. 1st ed. New York: Routledge. https://doi.org/10.1201/9780203747223.

Zeman, Leos, and Michael Wales. 1981. "Polymer Solute Rejection By Ultrafiltration Membranes." *ACS Symposium Series* II: 411–34. https://doi.org/10.1021/bk-1981-0154.ch023.

Zydney, Andrew L. 1992. "Concentration Effects on Membrane Sieving: Development of a Stagnant Filmmodel Incorporating the Effects of Solute-Solute Interactions." *Journal of Membrane Science* 68 (1–2): 183–90. https://doi.org/10.1016/0376-7388(92)80160-L.